From small scale variability to mesoscale stability in surface ocean pH: implications for air-sea CO_2 equilibration

Louise Delaigue[1,2], Gert-Jan Reichart[1,3], Li Qiu[4], Eric P. Achterberg[4], Yasmina Ourradi[1], Chris Galley[5,6], André Mutzberg[4] and Matthew P. Humphreys[1]

[1]Department of Ocean Systems (OCS), NIOZ Royal Netherlands Institute for Sea Research, PO Box 59, 1790 AB Den Burg (Texel), the Netherlands
[2]Sorbonne Université, CNRS, Laboratoire d'Océanographie de Villefranche, LOV, 06230 Villefranche-sur-Mer, France
[3]Department of Earth Sciences, Utrecht University, 3584 CS Utrecht, The Netherlands
[4]GEOMAR Helmholtz Centre for Ocean Research, Kiel, Germany
[5]Department of Earth Sciences, Memorial University of Newfoundland, St. John's, NL, A1B 3X5, Canada
[6]Department of Earth and Environmental Sciences, University of Ottawa, Ottawa, ON, K1N 6N5, Canada

Correspondence to: Louise Delaigue (louise.delaigue@imev-mer.fr)

Abstract. One important aspect of understanding ocean acidification is the nature and drivers of pH variability in surface waters on smaller spatial (i.e., areas up to 100 km^2) and temporal (i.e., days) scales. However, there has been a lack of high-quality pH data at sufficiently high resolution. Here, we describe a simple optical system for continuous high-resolution surface seawater pH measurements. The system includes a PyroScience pH optode placed in a flow-through cell directly connected to the underway supply of a ship through which near-surface seawater is constantly pumped. Seawater pH is measured at a rate of 2 to 4 measurements min^{-1} and is cross-calibrated using discrete carbonate system observations (total alkalinity, dissolved inorganic, carbon and nutrients). This setup was used during two research cruises in different oceanographic conditions: the North Atlantic Ocean (~~December–January~~ December 2020-January 2021) and the South Pacific Ocean (February-April 2022). By leveraging this novel high-frequency measurement approach, ~~O~~our findings reveal fine-scale fluctuations in surface seawater pH across the North Atlantic and South Pacific Oceans. While temperature is a significant abiotic factor driving these variations, it does not account for all observed changes. Instead, our results highlight the interplay between temperature, biological activity, and waters with distinct temperature-salinity properties~~water masses~~ on pH. Notably, the variability differed between the two regions, suggesting differences in the dominant factors influencing pH. In the South Pacific, biological processes appeared to be mostly responsible for pH variability, while in the North Atlantic, additional abiotic and biotic factors complicated the correlation between expected and observed pH changes. ~~Although surface seawater pH exhibited fine-scale variations, it remained relatively stable over a 24-hour cycle due to reequilibration with atmospheric CO_2. Thus, for the regions and time periods studied, ocean basin-scale analyses based on discrete samples collected during traditional research cruise transects would still capture the necessary variability for global CO_2 cycle assessments and their implications.~~ While our findings indicate that broader ocean-basin scale analyses based on lower-resolution datasets can effectively capture surface ocean CO_2 variability at a global scale, they also highlight the necessity of fine-scale observations for resolving regional processes and their drivers, which is essential for improving predictive models of ocean acidification and air-sea CO_2 exchange.

1 Introduction

Ocean chemistry is changing due to the uptake of anthropogenic CO_2 from the atmosphere (DeVries, 2022). The uptake of atmospheric CO_2 by the ocean's surface increases hydrogen ion concentration, a process known as ocean acidification, which has led to a 30–40% rise in hydrogen ion concentration (i.e. surface seawater acidity) and a corresponding pH decrease of ~0.1 since around 1850 ~~The uptake of atmospheric CO_2 by the ocean's surface causes a rise in the ocean's hydrogen ion concentration, a process commonly referred to as ocean acidification. As a result, the hydrogen ion concentration of surface ocean seawater has increased by 30–40%, which corresponds to a pH decrease of approximately 0.1 since around 1850~~ (Gattuso et al.,

Formatted: French (France)
Formatted: Subscript
Formatted: Subscript
Formatted: Subscript

2015; Jiang et al., 2019; Orr et al., 2005). These changes have already significantly impacted marine organisms, especially marine calcifiers (Doney et al., 2020; Gattuso et al., 2015; Osborne et al., 2020), and pH is projected to decline by ~0.3 by 2100 (Figuerola et al., 2021).

High-resolution studies of surface ocean carbonate chemistry and air-sea CO_2 exchange have significantly advanced our understanding of the upper ocean's carbon cycle.~~To understand these impacts and the underlying mechanisms more precisely, high-resolution studies have significantly advanced our understanding of the upper ocean's carbon cycle.~~ However, gaps remain, particularly at fine spatio-temporal scales (e.g., variability over hours and a few kilometers). At these scales, changes in pH over short time periods can be an important control on the ocean's buffering capacity and response to CO_2 uptake, highlighting the need for further detailed observations (Cornwall et al., 2013; Egilsdottir et al., 2013; James et al., 2020; Qu et al., 2017; Wei et al., 2022).

Formatted: Subscript

Advancements in the last decade and a half have enhanced the capacity for accurate and precise in-situ pH measurements. For example, Martz et al. (2010) developed an autonomous sensor tailored for continuous deployment in marine environments that allows recording of high-resolution pH fluctuations. Autonomous surface vehicles in coastal upwelling systems have also been used to capture intricate partial pressure of CO_2 (pCO_2) and pH dynamics, even in complex environments where rapid biogeochemical changes occur due to natural phenomena like upwelling (Chavez et al., 2018; Cryer et al., 2020; Possenti et al., 2021). Staudinger et al. (2018) also developed an optode system capable of simultaneously measuring oxygen, carbon dioxide, and pH in seawater. This system was designed for extended deployment (i.e. days) in marine environments, enabling continuous monitoring (with measurement intervals between 1 second and 1 hour) of these parameters. Additionally, Sutton et al. (2019) detailed the implementation of autonomous seawater pCO_2 and pH time series from 40 surface buoys, broadening the scope of observations at fixed time series sites. Staudinger et al. (2019) introduced fast and stable optical pH sensor materials specifically for oceanographic applications, enhancing the ability to measure pH under various environmental conditions.

These technological advancements have facilitated significant scientific progress. Field measurements conducted using submersible spectrophotometric sensors have revealed fine-scale variations in pH in coastal waters and shed light on localized acidification processes (Cornwall et al., 2013). The implementation of autonomous seawater pCO_2 and pH time series as described by Sutton et al. (2019) has enhanced our ability to characterize sub-seasonal variability in the ocean. These efforts represent important progress that can be built upon to further understand fine-scale ocean dynamics.

Fine spatio-temporal scale variability in surface ocean pH is hard to capture because it is driven by a complex interplay of processes, including physical mixing, biological activity (i.e. photosynthesis and respiration), thermal variability, and air-sea CO_2 fluxes (Faassen et al., 2023; Hofmann et al., 2011; Price et al., 2012). Physical mixing moderates surface oceanic pH by redistributing dissolved CO_2, nutrients, and heat throughout the water column. Mixing also mitigates extreme pH fluctuations by diluting surface concentrations of CO_2 during periods of high biological activity or temperature-induced CO_2 release (Egea et al., 2018; Li et al., 2019). Photosynthetic activity can decrease CO_2, leading to an increase in pH during daylight hours,

while respiration dominates at night, releasing CO_2 and lowering pH (Fujii et al., 2021; Jokiel et al., 2014). Warmer waters decrease CO_2 solubility and increase pH, while cooler waters increase solubility, promoting CO_2 uptake and decreasing pH, although the timescale of these processes differs, with some changes occurring instantaneously and others after equilibration (Zeebe & Wolf-Gladrow, 2001). Instantaneous changes are driven by physical and chemical reactions, while equilibration processes involve longer-term adjustments such as air-sea gas exchange and the mixing of surface waters with deeper layers (Emerson & Hedges, 2008). When atmospheric CO_2 exceeds oceanic CO_2, the ocean takes up CO_2, lowering pH; conversely, when atmospheric CO_2 decreases below oceanic CO_2, outgassing occurs, raising pH~~Increased atmospheric CO_2 boosts oceanic CO_2 uptake, lowering pH, while reduced atmospheric CO_2 would decrease oceanic CO_2, raising pH~~ (Caldeira & Wickett, 2005; Orr et al., 2005). Although each of these processes has its distinct impact on pH, their combined effects regulate the ocean's carbon cycle and its interaction with the atmosphere.

Recent studies on air-sea CO_2 equilibration timescales have highlighted significant regional variations, particularly between the North Atlantic and South Pacific Oceans (Jones et al., 2014). In the North Atlantic, equilibration timescales for CO_2 between the atmosphere and the ocean's surface mixed layer vary significantly with latitude. In regions above 55°N, these timescales can extend up to 18 months, while at lower latitudes, such as around 30°N, they range from 3 to 6 months ~~In the North Atlantic, deeper mixed layers and unstable oceanic conditions lead to longer equilibration timescales compared to temperate or tropical regions, ranging from 3 to 6 months for the average North Atlantic latitude, and up to 18 months for regions above 55 °N~~ (Jones et al., 2014). These long equilibration timescales reduce the extent to which the ocean can buffer short-term changes in surface pH. On pentadal and longer timescales, the air-sea CO_2 flux in the North Atlantic is driven primarily by changes in ΔpCO_2, while gas transfer velocity plays a more significant role only on interannual and shorter timescales (Couldrey et al., 2016).

Cooler temperatures at higher latitudes increase CO_2 solubility, resulting in higher dissolved inorganic carbon (DIC), and upwelling brings DIC and total alkalinity (TA)-rich deep waters to the surface (Wu et al., 2019). These factors further increase the amount of CO_2 that needs to ~~equilibrate~~ exchange with the atmosphere, further prolonging equilibration times. The South Pacific, with its shallower mixed layers and higher average surface temperatures, facilitates shorter equilibration times and enhances CO_2 uptake rates (i.e. 3 to 4 months; Jones et al., 2014). Wu et al. (2019) also showed that high biological productivity in these areas significantly impacts DIC, potentially reducing surface DIC more quickly.

Here, we test a high-frequency optical system to investigate how surface seawater pH varies across fine spatio-temporal scales, focusing on changes occurring over areas up to 100 km^2 and timescales of hours to days~~Here, we investigate how surface seawater pH varies on fine spatio-temporal scales (i.e areas up to 100 km^2, and days)~~ across different ocean basins (i.e., North Atlantic and South Pacific Oceans) and identify abiotic and biotic factors driving these variations. We use direct, high-frequency measurements of surface seawater pH and estimate TA to resolve the rest of the carbonate system. This novel setup provides new insights into ~~. These data are used to analyse how key biogeochemical~~ processes, such as temperature, hydrodynamic mixing and biological activity, influence fine-scale spatio-temporal variability in pH.

Formatted: Subscript

Formatted: Subscript

Formatted: Subscript

Formatted: Subscript

Formatted: Superscript

Formatted: Font: Not Bold

Formatted: Font: Not Bold

2 Materials and Procedures

2.1 Study areas

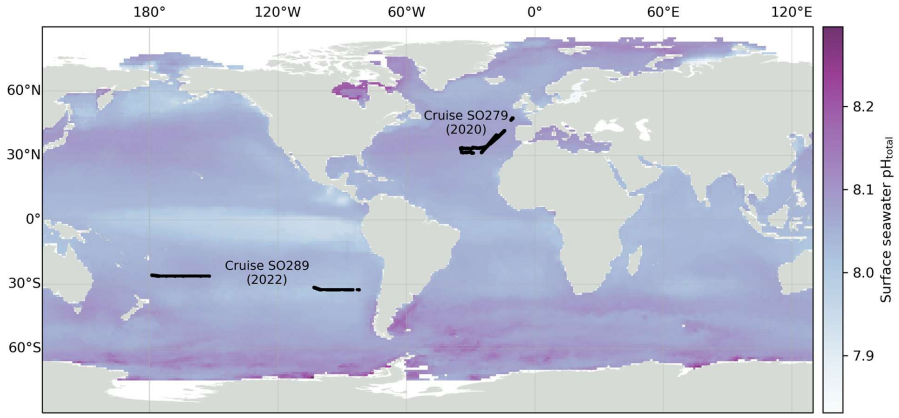

Figure 1. Locations of pH measurements during two oceanographic cruises used in this study: SO279 in the North Atlantic (December 2020 to January 2021) and SO289 in the South Pacific (February-April 2022). Surface seawater pH on the total scale ~~pH$_{total}$~~ for December 2022 from the OceanSODA product is shown in the background (Gregor & Gruber, 2020).

Two datasets from separate oceanic regions were used: research expeditions SO279 in the North Atlantic Ocean and SO289 in the South Pacific Ocean, both on the German R/V Sonne (Fig. 1).

Expedition SO279 in January to December 2020, conducted in the Azores Region of the North Atlantic Ocean (Fig. 1), was part of the NAPTRAM research program investigating the transport pathways of plastic and microplastic debris (Beck et al., 2021). The data collection included discrete samples from the CTD rosette (n=77; (Delaigue et al., 2021a), with measurements of DIC, TA and nutrients (silicate, phosphate ammonium, nitrite, and nitrate + nitrite); discrete samples from the underway water system (UWS; n=51; (Delaigue et al., 2021b) also measuring these parameters; and a high-resolution UWS timeseries of ocean surface pH (over 43,000 datapoints; (Delaigue et al., 2021c).

The South Pacific GEOTRACES Cruise SO289, from Valparaiso (Chile) to Noumea (New Caledonia) under the GEOTRACES GP21 initiative, was conducted from ~~between 18~~ February ~~and 08~~ to April 2022 (Fig. 1; (Achterberg et al., 2022). The data collection also included ~~discrete carbonate chemistry and nutrient samples~~the same parameters as SO279, ~~from the~~ with discrete samples from the CTD rosette (n=395; (Delaigue, Ourradi, Ossebar, et al., 2023), discrete samples from the UWS (n=32; (Delaigue, Ourradi, et al., 2023a) and another high-resolution UWS timeseries of ocean surface pH from the optode system (over 78,000 datapoints; (Delaigue, Ourradi, et al., 2023b).

2.2 Integrated ~~Shipboard~~ shipboard ~~O~~optode ~~S~~system for ~~C~~continuous pH ~~M~~measurements

We used a pH optode (PHROBSC-PK8T, for pH range 7.0 – 9.0 on the total scale; PyroScience GmbH), made of a robust cap adapter fiber with a stainless-steel tip (length=10cm, diameter=4mm) and disposable plastic screw cap with an integrated pH sensor. The total scale accounts for sulfate ion dissociation in seawater, providing a more accurate representation of carbonate system equilibria compared to other pH scales commonly used in marine chemistry. Unless explicitly stated otherwise, all references to pH in this manuscript refer to pH on the total scale. The manufacturer-reported accuracy of the optode is ±0.05 for pH 7.5–9.0 and ±0.1 for pH 7.0–7.5 after a two-point calibration, with a precision of ±0.003 at pH 8.0.

~~-~~The optode was connected to a meter combined with a pressure-stable optical connector (optical feed-through; OEM module Pico-pH-SUB; PyroScience GmbH; Fig. 2). Briefly, the optical pH sensor is constructed using the PyroScience REDFLASH technology, which uses a pH neutral reference indicator and a pH responsive luminescent dye. These elements are activated using a specifically tuned orange-red light with a wavelength ranging between 610-630 nm, which triggers a bright luminescence emission in the near-infrared (NIR) band, spanning from 760-790 nm. At elevated pH, the fluorescence from the pH marker is diminished, leaving only the NIR emission of the reference indicator noticeable. As the acidity increases, the pH marker is protonated, which results in a heightened NIR luminescence that is detected along with the emissions of both indicators. The measurement approach uses red excitation light modulated in a sinusoidal manner, leading to a similar modulation of the NIR emission, albeit with a phase discrepancy. This phase variation is registered by the PyroScience OEM module and subsequently converted into a total pH measurement.

Automatic temperature compensation of the optical pH sensor was achieved using a flexible Teflon-coated temperature probe (Pt100 Temperature Probe, PyroScience GmbH; Fig. 2) soldered onto the OEM module. The optode was placed in a closed flow-through cell directly connected to the underway supply of the ship through which seawater was pumped at a constant rate (6 L/min for SO279 and 9 L/min for SO289; 2.5 m depth) and stirred using a magnetic stirrer (Fig. 2). The entire setup was kept inside a closed box to isolate the optical instrument from any other light source (Fig. 2). All seawater first went through a thermo-salinograph close to the water source, which also measured salinity, temperature and chlorophyll-a fluorescence (chl-a), before going through the pH setup (Fig. 2).

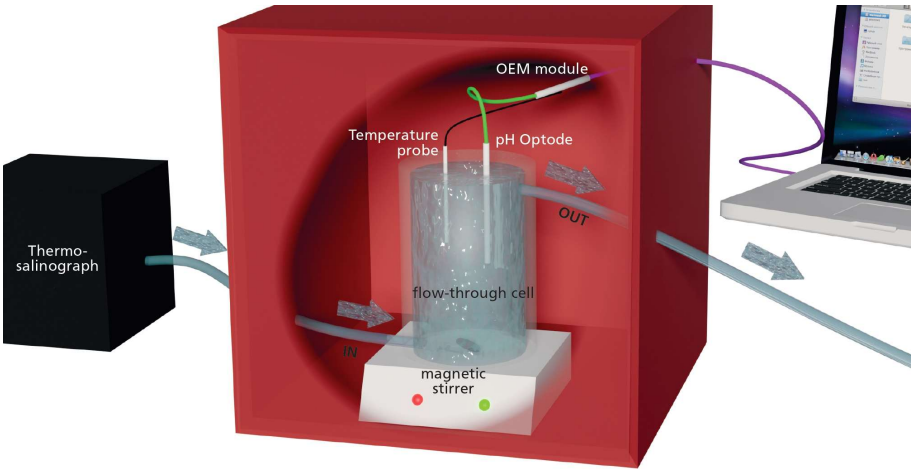

Figure 2. Schematic representation of the optical continuous pH measurement system. Arrows indicate the direction of flow-through tubing. The system consists of the following components: a thermo-salinograph; a flow-through cell; a magnetic stirrer; a fiber-based pH optode; a flexible Teflon-coated temperature probe; a fiber-optic meter OEM module Pico-pH-SUB and a portable computer. All elements inside the red box are in the dark to avoid any light disturbance.

2.3 Initial calibration and underway measurements

Direct measurements of surface water (~3 m depth) pH were carried out at a frequency of 2 measurements min^{-1} for the North Atlantic cruise and 4 measurements min^{-1} for the South Pacific cruise.

A one-point calibration of the temperature probe was performed against a thermometer inside a water bath (Lauda Ecoline RE106). A two-point calibration of the pH sensor was ~~performed~~ conducted following the manufacturer's recommended procedure, using PyroScience pH buffer capsules (pH 2 or pH 4 for the acidic calibration point, pH 10 or pH 11 for the basic calibration points). ~~While t~~These calibration points deliberately fall far outside the sensor's operating range from pH 7-9 in order to characterize its maximum and minimum responses~~are far from typical surface ocean pH (~8.1), this approach ensures sensor linearity across its operational range (pH 7.0–9.0) and follows the manufacturer's specifications~~. Buffers were prepared by dissolving each capsule's powder into 100 mL MilliQ water.

~~A pH offset adjustment was made using certified reference material (CRM, batches #189, #195 and #198; provided by Andrew Dickson, Scripps Institution of Oceanography).~~

To further refine the accuracy of the measurements, a pH offset adjustment was applied using certified reference material (CRM, batches #189, #195, and #198; provided by Andrew Dickson, Scripps Institution of Oceanography). Although CRMs do not provide direct certified pH values, we calculated pH_{CRM} from the CRM TA and DIC using the carbonate system equilibrium constants from Lueker et al. (2000). This pH_{CRM} value was then used to adjust the optode-based pH measurements to improve accuracy and align them with discrete observations.

Formatted: Font: Not Bold

Formatted: Font: Not Bold

Formatted: Font: Not Bold

Formatted: Subscript

Formatted: Font: Not Bold

Formatted: Font: Not Bold

Formatted: Subscript

Formatted: Font: Not Bold

To assess the robustness of the pH optode, resolution surface measurements of partial pressure of CO_2 (pCO_2) and pH (samipH) were added as points of comparison. The pH optode, pCO_2 sensor, and samipH sensor were all installed on the same surface seawater supply, which was continuously pumped from approximately 2.5 m depth into the sink of the underway laboratory during the cruise. The PyroScience pH sensor received water from a split of this same supply, ensuring all sensors were sampling the same source water.

Surface pCO_2 was measured using a factory-calibrated commercial sensor (HydroC, 4H-JENA Engineering GmbH, Germany)(Fietzek et al., 2014) at a 1-minute sampling interval. An automatic zero-point calibration was performed every 6 hours to correct for sensor drift. The recorded pCO_2 values were subsequently adjusted following (Takahashi et al., 2006) to reflect in situ sea surface temperature.

Surface pH, reported on the total scale, was measured using a factory-calibrated sensor (Sunburst Sensors, USA) at 15-minute intervals. The pH data were calibrated using sea surface salinity and temperature according to the equations provided by Liu et al. (2011) and Millero (2007), respectively.

Formatted: Subscript

Formatted: Subscript

Formatted: Subscript

2.4 Discrete sampling and analysis for other CO_2 parameters

The underway seawater system was sub-sampled from the cell every 12 hours via silicone tubing for TA and DIC following an internationally established protocol (Dickson et al., 2007). TA was sampled in Azlon™ HDPE wide neck round 150 mL bottles filled to the neck and poisoned with 50 µL saturated $HgCl_2$. DIC was sampled into Labco Exetainer® 12 ml borosilicate vials and poisoned with 15 µL saturated $HgCl_2$. Samples were stored at 4 °C whenever possible and kept in the dark until analysis.

All TA and DIC analysis was carried out at the Royal Netherlands Institute for Sea Research, Texel (NIOZ). The analysis was calibrated using certified reference material (CRM, batches #189, #195 and #198; provided by Andrew Dickson, Scripps Institution of Oceanography). TA was determined using a Versatile INstrument for the Determination of Total inorganic carbon and titration Alkalinity (VINDTA 3C #017 and #014, Marianda, Germany). The instrument performed an open-cell, potentiometric titration of a seawater subsample with 0.1 M hydrochloric acid (HCl). Results were then recalculated using a modified least-squares fitting as implemented by Calkulate v3.1.0 (Humphreys and Matthews, 2024). DIC concentrations were determined using either the VINDTA system (SO279 samples and part of SO289 samples) or the QuAAtro Gas Segmented Continuous Flow Analyzer (CFA, SEAL Analytical; SO289 samples). Briefly, the VINDTA measures DIC by acidifying a seawater sample, which releases CO_2 that is then quantified through a coulometric titration cell. Similarly, the QuAAtro CFA uses acidification to liberate CO_2, which then discolours a slightly alkaline phenolphthalein pink coloured solution which is measured spectrophotometrically at 520 nm (Stoll et al., 2001).

For cruise SO279, nutrient samples were gathered using 60 mL syringes made of high-density polyethylene, which were connected to a three-way valve by tubing, drawing directly from the CTD-rosette bottles to avoid air exposure. Immediately upon collection, the samples were taken to the laboratory for processing, where they were filtered through a dual-layer filter with pore sizes of 0.8 and 0.2 µm. All samples were stored at -20°C in a freezer except Si, which were

stored at 4°C in a cold room until analysis back at NIOZ. Nutrients were analysed using a QuAAtro Continuous Flow Analyser. Measurements were made simultaneously on four channels together Si, PO_4, NH_4, NO_3, and NO_2. All measurements were calibrated with standards diluted in low nutrient seawater (LNSW) in the salinity range of the stations (approx. 34 – 37) to ensure that analysis remained within the same ionic strength. Prior to analysis, all samples were brought to laboratory temperature in about one to two hours. To avoid gas exchange and evaporation during the runs with NH_4 analysis, all vials including the calibration standards were covered with Parafilm under tension before being placed into the auto-sampler, so that the sharpened sample needle easily penetrated through the film leaving only a small hole. Silicate samples were measured separately on a TRAACS Gas Segmented Continuous Flow Analyser (manufactured by Bran+Lubbe, now SEAL Analytical) following Strickland and Parsons (1972). A sampler rate of 60 samples per hour was also used for all analyses. Calibration standards were diluted from stock solutions of the different nutrients in 0.2 µm filtered LNSW diluted with de-ionised water to obtain approximately the same salinity as the samples and were freshly prepared every day. This diluted LNSW was also used as the baseline water for the analysis and in between the samples. Each run of the system had a correlation coefficient of at least 0.9999 for 10 calibration points. The samples were measured from the lowest to the highest concentration, i.e., from surface to deep waters in order to reduce carry-over effects. Concentrations were recorded in µM at an average container temperature of 23.0 °C and later converted to µmol/kg by dividing the recorded concentration by the sample density, calculated following Millero and Poisson (1981).

For cruise SO289, nutrient analysis was carried out on seawater from every Niskin bottle triggered at various depths during each cast. The seawater was transferred into 15 mL polypropylene vials. Each container and its cap were rinsed three times with seawater before filling. If immediate analysis was not possible, samples were stored in a fridge at 4 °C in the dark. Macro nutrients were analyzed onboard using a segmented flow injection analysis with a Seal Analytical QUAATRO39 auto-analyzer that includes an XY2-autosampler. For nanomolar nutrient analysis, a modified setup with 1000 mm flow cells was employed. The setup was designed to analyze four channels: total oxidized nitrogen (TON), silicate, nitrite, and phosphate, using methods outlined in QuAAtro Applications: Method Nos. Q-068-05 Rev. 11, Q-066-05 Rev. 5, Q-070-05 Rev. 6, and Q-064-05 Rev. 8, respectively. To ensure analytical consistency and validate the data, each run was checked against Certified Reference Material for Nutrients in Seawater (RMNS). Nutrient analyses were further validated using KANSO CRM, with specific lot numbers for macromolar and nanomolar nutrient concentrations.

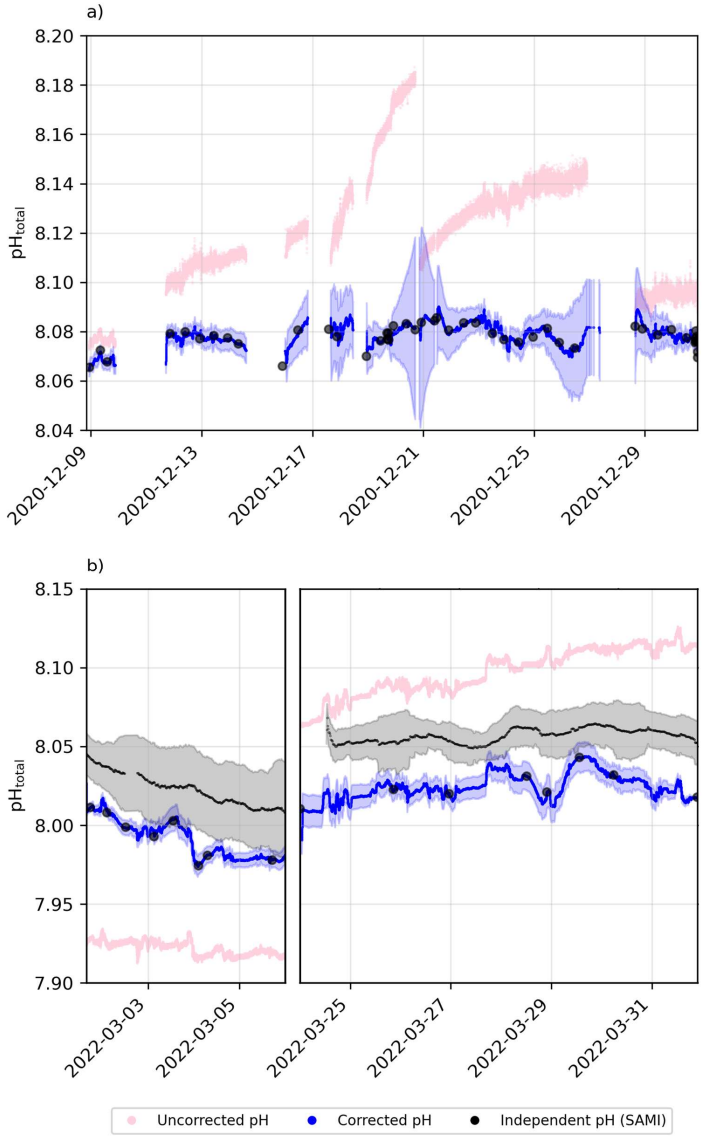

Figure 3. Underway pH drift correction using $pH_{total(TA/DIC)}$ subsamples for a) cruise SO279 and b) cruise SO289. Raw pH measurements (pink); corrected pH values and uncertainty from bootstrapping (blue); subsample $pH_{total(TA/DIC)}$ depicted as black circles. Independent pH from the SAMI sensor is shown in black for the South Pacific cruise (SO289).

2.5 Post-cruise correction

To ensure the reliability of the dataset, an initial screening was conducted to identify and flag unreliable continuous pH data points, primarily attributable to optode stabilization issues. Specifically, data points recorded during documented periods of particularly ~~high seas~~rough weather, when air intrusion into the underway system was reported, were flagged as unreliable due to the resulting abrupt and erratic drift patterns inconsistent with expected optode and surface ocean pH behavior.~~Specifically, data points exhibiting unreasonable drift patterns, inconsistent with expected optode and surface ocean pH behavior, were flagged as unreliable.~~

pH_{obs}~~$_{TA, DIC}$~~ ~~values~~ was~~ere~~ calculated from TA and DIC UWS discrete samples) using PyCO2SYS (Version 1.8.2; (Humphreys et al., 2022)), with the carbonic acid dissociation constants of Lueker et al. (2000), the bisulfate dissociation constant of Dickson (1990), the total boron to chlorinity ratio of Uppström (1974), and the hydrogen fluoride dissociation constant of Dickson and Riley (1979). ~~Lueker et al. (2000)~~These calculated values were then aligned with the continuous pH dataset to determine the offset between pH_{obs} subsamples and the continuous optode-based pH measurements (Fig. 3).~~and were then aligned with the continuous pH data to calculate the offset between the $pH_{TA, DIC}$ subsamples and the continuous pH data (Fig. 3).~~ A Piecewise Cubic Hermite Interpolating Polynomial (PCHIP; (Fritsch & Carlson, 1980) was fitted to the offset as a way to continuously correct pH variations across the entire pH timeseries (Fig. 3). While continuous recalibration of the optode was not possible, a two-point calibration, supplemented by a third-point correction using a CRM, was performed prior to deployment (see Section 2.3). Additionally, discrete underway TA and DIC samples, collected twice daily when possible, were used to assess and correct for drift in the optode measurements. ~~However, it appears that the sensor drifted significantly faster than this, so over timescales of days and longer the accuracy of the measurement is dependent on the correction to the TA and DIC samples~~ The manufacturer specifies a drift of <0.005 pH units per day at 25 °C, though drift may vary slightly with temperature. During our deployments, seawater temperatures ranged from 13.4°C to 22.0 °C in the North Atlantic and from 19.8°C to 27.7 °C in the South Pacific. While the cooler North Atlantic conditions may have reduced drift rates slightly, temperatures during the South Pacific cruise were close to or above 25 °C for extended periods, and full manufacturer-specified drift is likely to have occurred. Even if drift remained at the nominal rate of 0.005 pH units per day, this would amount to a cumulative offset of up to 0.175 pH units over ~5 weeks (SO279) and 0.28 pH units over ~8 weeks (SO289), in line with the deviation observed in our raw data (Fig. 3). Notably, even with a recalibration during the cruise, drift before and after that point would still introduce offsets. Thus, over timescales of days and longer, the accuracy of the measurement is dependent on the correction to the TA and DIC samples.

To further assess the robustness of our drift correction, we compared our optode-corrected pH and derived fCO_2 values with independent continuous measurements from autonomous sensors (Figs. S1 and S2). The corrected optode pH exhibited a lower mean deviation (~0.008) from discrete pH (TA/DIC) measurements than the independent spectrophotometric SAMI sensor (~0.02 pH units), indicating that our correction effectively minimized drift-related inaccuracies (Fig. S1). The overall scatter between the optode-corrected and SAMI-measured pH was modest (RMSD = 0.0329), suggesting reasonable consistency despite inherent sensor measurement noise. Similarly, calculated fCO_2 from corrected optode pH showed a larger mean deviation (~12.7 µatm) compared to directly measured fCO_2 (~5 µatm; Fig. S2). The relatively higher

Formatted: Subscript

Commented [LD1]: CG: Best to avoid brackets within brackets.

Commented [LD2R1]: This will be fixed one I get rid off the EndNote formatting!

Formatted: Subscript

Formatted: Not Highlight

Formatted: Not Highlight

Formatted: Not Highlight

RMSD (30.76 µatm) reflects variability in calculated fCO_2 arising from uncertainties in alkalinity estimates and carbonate system calculations rather than fundamental flaws in the optode pH correction itself (Fig. S2). Thus, these validations collectively confirm that our corrected pH data represent a reliable improvement over raw optode measurements, suitable for robust biogeochemical analysis.

The overall post-cruise correction of pH involved an adjustment of approximately 0.4 to bring the continuous measurements in line with discrete carbonate system observations. However, despite this magnitude of correction, the internal variability within each cycle remains robust, with observed diel fluctuations consistently within ~0.01. This fine-scale variability aligns with expected temperature-driven pH changes and is distinguishable from random noise. The measurement uncertainty of ~ ±0.01 means that while some small-scale variations approach the uncertainty threshold, the structured nature of the observed diel trends—rather than random scatter—supports their validity. If these variations were purely noise, we would not expect to see systematic agreement with temperature fluctuations across multiple cycles and regions. To further assess the robustness of these signals, we conducted a signal-to-noise ratio (SNR) analysis (see Supplementary Information). SNR values exceeded 1 when pH was modeled based on temperature (and salinity) in the North Atlantic, indicating that observed diel variability surpassed measurement noise and reflected true environmental signals. In contrast, SNR values remained below 1 in the South Pacific, suggesting that pH variability there was closer to the uncertainty threshold and less clearly distinguishable from noise.

2.6 Estimation of other biogeochemical parameters

TA was estimated for the continuous pH dataset using the empirical equations presented by Lee et al. (2006). For the North Atlantic, the corresponding equation was used (see Fig. S3~~1~~ in supplementary information):

$$TA_{NA} = 2305 + 53.97(SSS - 35) + 2.74(SSS - 35)^2 - 1.16(SST - 20) + 0.040(SST - 20)^2 \quad (1)$$

In contrast, the (Sub)tropics equation (SBT, Eq. 2) was applied for the South Pacific region, as the cruise mostly followed the 32.5°S longitude and this equation was determined to offer the best fit to the local temperature (SST) and salinity (SSS) equation (see Fig. S~~1~~3 in supplementary information):

$$TA_{SBT} = 2305 + 58.66(SSS - 35) + 2.32(SSS - 35)^2 - 1.41(SST - 20) + 0.040(SST - 20)^2 \quad (2)$$

TA estimates were used together with pH to solve the rest of the marine carbonate system (i.e. DIC and fCO_2) using PyCO2SYS (Version 1.8.2; (Humphreys et al., 2022), with the carbonic acid dissociation constants of Lueker et al. (2000), the bisulfate dissociation constant of Dickson (1990), the total boron to chlorinity ratio of Uppström (1974), and the hydrogen fluoride dissociation constant of Dickson and Riley (1979).

While direct TA measurements were collected twice daily, their limited temporal resolution made them unsuitable for continuous carbonate system calculations. The empirical TA equations

Formatted: Not Highlight

Commented [LD3]: MPH: are they the Lee eq or did I refit them to my data? Did I check this against my TA data?

Commented [LD4R3]: No I just used the Lee et al equations given data is in the open ocean for both regions

from Lee et al. (2006) provided a high-resolution dataset that allowed for more comprehensive system reconstructions. A comparison of measured and estimated TA values (see Fig. S3 in supplementary information) shows good agreement, with deviations generally within the uncertainty of carbonate system calculations.

2.7 Projected pH variability

The derived parameters pH_{temp}, pH_{sal}, and $pH_{temp,sal}$ were calculated while holding TA and DIC constant at the average values of each ~~diurnal~~diel cycle, where TA was estimated following Lee et al. (2006) and DIC was derived from measured underway pH and estimated TA. This approach allowed us to assess the expected pH response to changes in temperature and salinity alone, without introducing additional assumptions about concurrent variations in carbonate chemistry.

Similarly, $pH_{TA,fCO2}$ was computed while holding TA and fCO_2 constant at their daily mean values. fCO_2 was derived from measured pH and estimated TA, ensuring that the calculation reflects equilibrium conditions for given waters with distinct temperature-salinity properties while allowing temperature and salinity to vary independently. This formulation enables direct comparisons of observed pH to expected values under different scenarios, helping to disentangle the relative influences of abiotic drivers (temperature, salinity) versus processes such as air-sea CO_2 exchange and biological activity.

Our approach maintains consistency by using a single set of carbonate chemistry parameters (TA and DIC) as the baseline for assessing temperature and salinity influences. While pH is initially used to estimate DIC, the subsequent calculations isolate the effects of temperature and salinity without assuming variability in TA or DIC. This method enables direct comparisons between observed and expected pH, providing a clearer framework for distinguishing abiotic influences from biological processes and air-sea CO_2 exchange.

~~These calculations allowed for the exploration of changes in pH under varying environmental conditions by solely altering either temperature, salinity, or both simultaneously. $pH_{TA,fCO2}$ was also computed while holding TA and fCO_2 constant at their daily mean values but with varying temperature and salinity to model the pH distribution under fully equilibrated conditions.~~ All calculations were done using the same ~~options~~ configuration in PyCO2SYS described in Sect. 2.6.

2.8 Identification of full ~~diurnal~~diel ~~-~~diel cycles

To account for the influence of geographic location on temporal measurements, timestamps from Coordinated Universal Time (UTC) were converted to Local Solar Time (LST). This conversion was necessary to align time-sensitive data with the true solar position at each measurement location, thereby facilitating more accurate comparisons of environmental data across different geographic regions and improving the analysis of ~~diurnal~~diel-diel processes.

The conversion process involved calculating the mean longitudinal position for each date within the dataset. Subsequently, a time offset was determined based on the average longitude, assuming a standard rate of Earth's rotation. This offset was then applied to the original UTC timestamps, resulting in a modified dataset with timestamps adjusted to reflect LST:

Formatted: Font: Not Bold

Formatted: Subscript

Formatted: Font: Italic

Formatted: Subscript

Formatted: Font: Italic

Formatted: Subscript

Formatted: Subscript

Formatted: Subscript

$$\mathrm{DateTime_{LST}} = \mathrm{DateTime_{UTC}} + \left(\frac{\mathrm{Longitude_{mean}}}{15}\right). \quad (3)$$

Following the conversion to LST, the dataset was further processed to isolate complete ~~diurnal~~diel cycles to ensure that only data representing full 24-hour cycles were included. The North Atlantic dataset included 7 complete ~~diurnal~~diel cycles, while the South Pacific dataset included 11 complete ~~diurnal~~diel cycles.

2.9 Uncertainty propagation

2.9.1 Uncertainty in pH measurements and post-correction

To provide a comprehensive uncertainty estimate, we considered multiple sources of potential error. The manufacturer-reported accuracy (±0.05 for pH 7.5–9.0, ±0.1 for pH 7.0–7.5) represents a systematic bias that was addressed through calibration against discrete CRM samples and is not appropriate for inclusion as a random uncertainty. Likewise, the reported precision (±0.003 at pH 8.0) reflects the repeatability of the measurements but does not quantify the full range of uncertainty for error propagation. The final uncertainty in pH measurements was estimated by combining uncertainties from two main sources: (1) the uncertainty in the TA and DIC measurements used to calculate $pH_{obs(TA/DIC}$ and (2) the correction of the UWS pH measurements using $pH_{obsTA, DIC.}$

First, the precision in TA and DIC were determined based on the RMSE from repeated measurements of a known standard water sample in the laboratory (NIOZ; 0.92 umol/kg and 1.95 µmol/kg, respectively). Then a Monte Carlo simulation was applied to the calculated $pH_{obsTA, DIC}$ to obtain a pH_{RMSE} for each subsample $pH_{obsTA, DIC}$.

Next, the pH measurements obtained from the optode were corrected using $pH_{(TA, DIC)}$ from the discrete measurements of TA and DIC. The uncertainty in the pH correction was assessed using a bootstrapping approach (n=1000 iterations), where a fraction (50%) of the discrete samples was randomly omitted in each iteration and the selected fraction of the discrete samples varied within its own pH_{RMSE}.

The variation in each subsample's $pH_{obsTA, DIC}$ captured the likely variability in TA and DIC measurements, while omitting different subsets of data allowed for the estimation of how sensitive the pH correction is to which set of subsamples are used for calibration.

2.9.2 Uncertainty in pH ~~diurnal~~diel patterns

To ensure the observed patterns in pH over the full 24-hour cycles were not artifacts of sampling bias or other anomalies, a Monte Carlo simulation (n = 1000 iterations) was employed on each ~~diurnal~~diel cycle's hourly data analysis. This simulation randomly selected 50% of the data points for each hour (i.e. 50% of 120 hourly measurements for the North Atlantic dataset and 50% of 240 hourly measurements for the South Pacific dataset), repeatedly calculating the mean pH to assess the consistency and robustness of the hourly trends. This component of the uncertainty proved insignificant (i.e., errors bars were smaller than the symbols in Fig. 4 and 5).

Formatted: Subscript

Formatted: Subscript

Formatted: Subscript

Formatted: Subscript

2.10 CO_2 air-sea flux dynamics

~~The difference in pCO_2 between the air and ocean surface dictates the direction of gas exchange and determines whether the ocean acts as a CO_2 source or sink to the atmosphere. This CO_2 exchange between the air and sea, referred to as~~ Air-Sea CO_2 flux~~, can be~~ were computed based on the relationship:

$$F = k_w \times K_0 \times (pCO_{2_{SW}} - pCO_{2_{air}}) \quad (4)$$

where F represents the flux of CO_2 across the air-sea interface, k_w is the gas transfer velocity, K_0 is the solubility constant and $pCO_{2_{SW}}$ is the partial pressure of CO_2 in sea water, representing the concentration of dissolved CO_2 that is in equilibrium with the atmosphere and $pCO_{2_{air}}$ is the partial pressure of CO_2 in the atmosphere above the ocean surface. For the fluxes, a positive value shows the ocean acts as a source (i.e., releasing CO_2 to the atmosphere), while a negative value shows it acts as a sink (i.e., absorbing CO_2 from the atmosphere). The parameterisation from Ho et al. (2006) was used to determine the gas transfer velocity. All fluxes were computed using the pySeaFlux package (v2.2.2; (Fay et al., 2021).

Flux calculations were performed for each complete ~~diurnal~~diel cycle, followed by the computation of the mean flux for each cycle. Additionally, the mean flux for the ~~diurnal~~diel cycle was also calculated from the daily mean inputs (wind speed, temperature, salinity, and pCO_2), and specifically computed for the hours 12 AM and 12 PM (LST) to examine temporal variations within each cycle (Fig. 9).

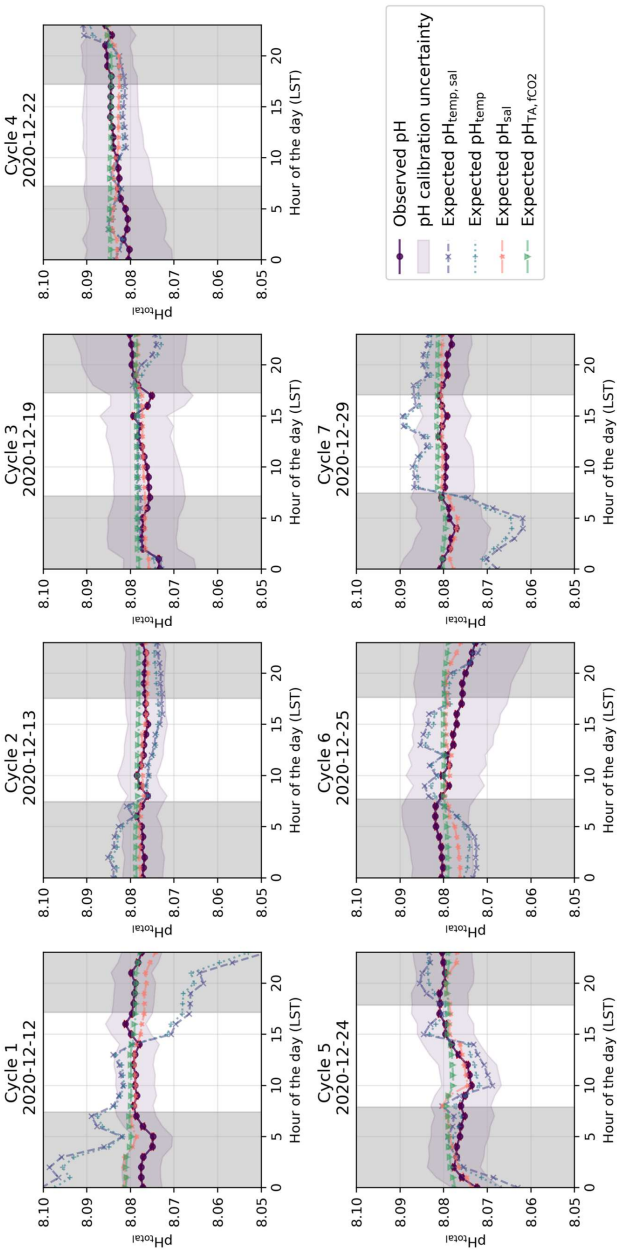

Figure 4. Identified diel cycles for cruise SO279 in the North Atlantic Ocean. Dark purple lines show observed pH (pH$_{obs}$), dashed grey lines show mean observed pH over the full diel cycle, and black lines show overall mean pH for all diel cycles combined for that cruise. The remaining shows expected pH using varying temperature and salinity (pH$_{temp,sal}$; dashed light purple lines), varying temperature alone (pH$_{temp}$; dashed blue lines), varying salinity alone (pH$_{sal}$; dashed orange lines) and constant TA and fCO_2 (pH$_{TA,fCO2}$; dashed green lines). Grey areas are night hours.

~~**Figure 4. Identified diurnaldiel cycles for cruise SO279 in the North Atlantic Ocean. Dark purple lines show observed pH, dashed grey lines show mean observed pH over the full diurnaldiel cycle, and black lines show overall mean pH for all diurnaldiel cycles combined for that cruise. The remaining shows expected pH using constant TA and DIC (averaged for each respective diurnaldiel cycle) and varying temperature and salinity (dashed light purple lines), varying temperature alone (dashed blue lines), varying salinity alone (dashed orange lines) and constant TA and fCO_2 (dashed green lines). Grey areas are night hours.**~~

506

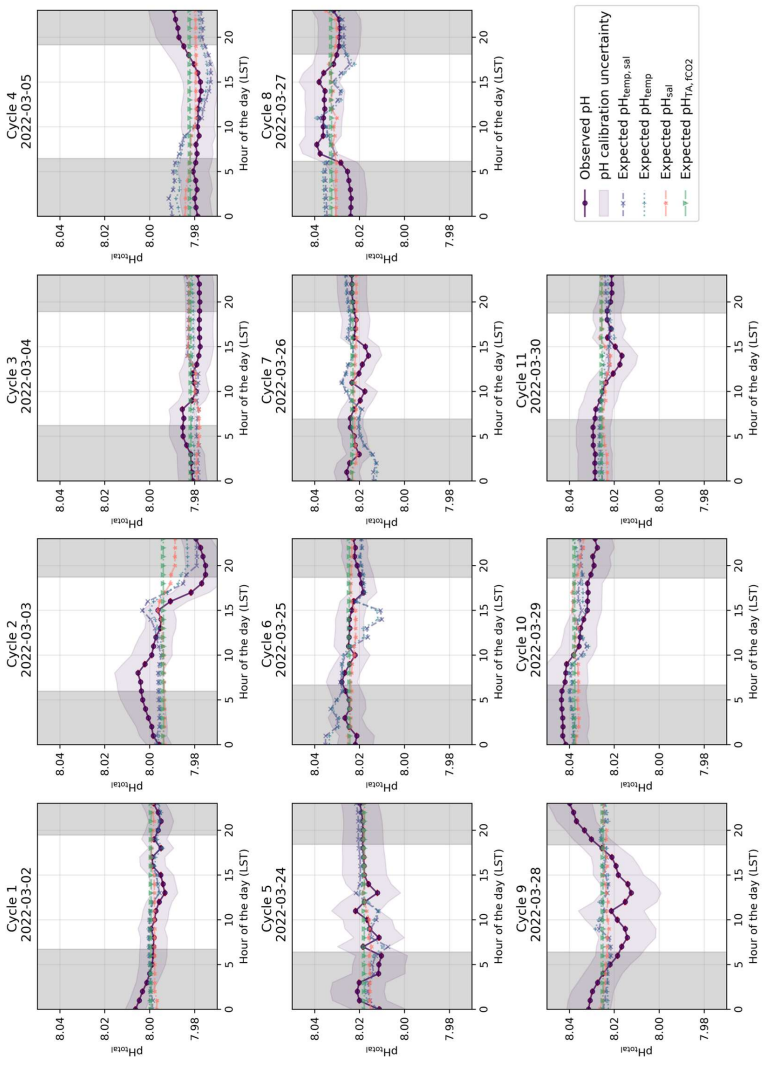

Figure 4. Identified diel cycles for cruise SO289 in the South Pacific Ocean. Dark purple lines show observed pH (pH_{obs}), dashed grey lines show mean observed pH over the full diel cycle, and black lines show overall mean pH for all diel cycles combined for that cruise. The remaining shows expected pH using varying temperature and salinity ($pH_{temp,sal}$; dashed light purple lines), varying temperature alone (pH_{temp}; dashed blue lines), varying salinity alone (pH_{sal}; dashed orange lines) and constant TA and fCO_2 ($pH_{TA,fCO2}$; dashed green lines). Grey areas are night hours.

~~**Figure 5. Identified diurnaldiel cycles for cruise SO289 in the South Pacific Ocean. Dark purple lines show observed pH, dashed grey lines show mean observed pH over the full diurnaldiel cycle, and black lines show overall mean pH for all diurnaldiel cycles combined for that cruise. The remaining shows expected pH using constant TA and DIC (averaged for each respective diurnaldiel cycle) and varying temperature and salinity (dashed light purple lines), varying temper (dashed blue lines), varying salinity alone (dashed orange lines) and constant TA and fCO2 (dashed green lin night hours.**~~

Commented [LD5]: Intercomparison of cycles --> calibration error is important

Intercomparison of hours --> maybe there is uncertainty in the hourly means too / maybe not significant but this needs to be at least mentioned in the discussion

Eg. Monte Carlo --> doing the hourly mean using different amounts of points (max 120 per hour) for example taking 60 points at random for one hour and doing it 1000 times --> that's a different error, that's the error in the trend, not in the absolute values / can indicate it with a different color of fill_between or even as small error bars

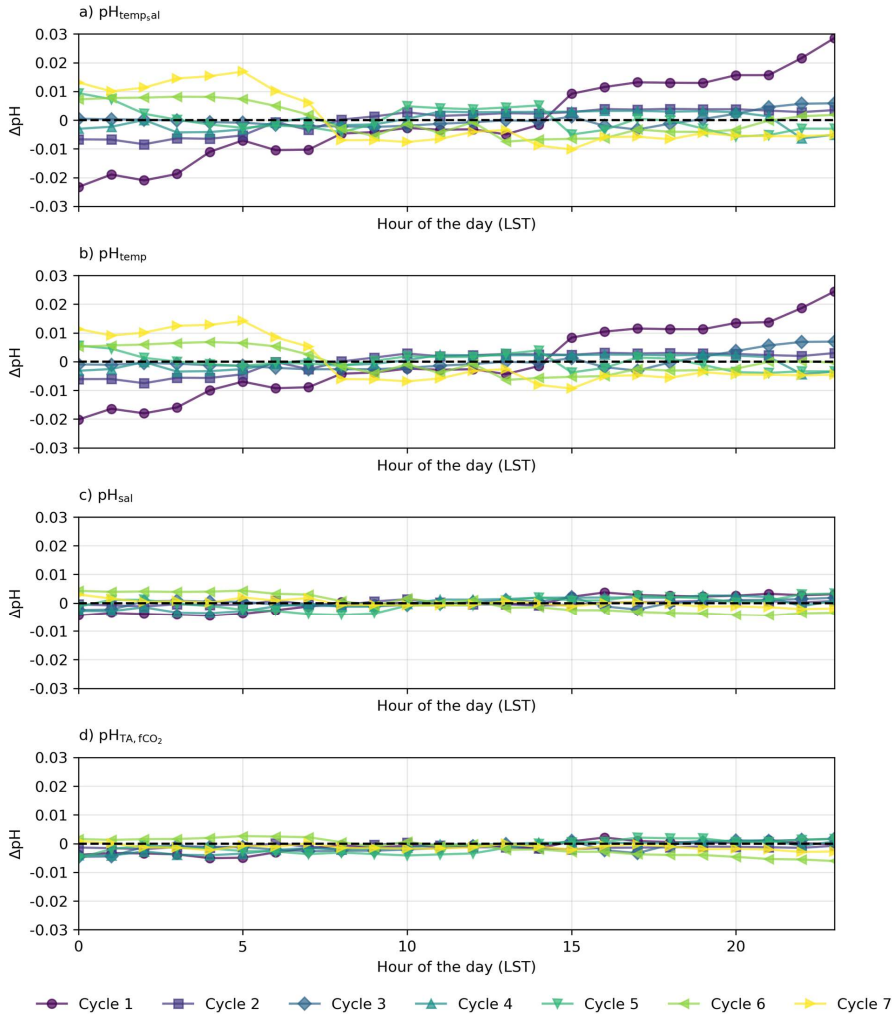

Figure 6. Residual plots for ~~diurnal~~diel cycles in the North Atlantic, illustrating the ~~discrepancies~~differences (ΔpH) between observed pH measured by the optode (pH$_{obs}$) and a) pH calculated from constant TA and DIC with varying temperature and salinity (pH$_{temp,sal}$), b) varying temperature only (pH$_{temp}$), c) varying salinity only (pH$_{sal}$) and d) constant TA and fCO_2 with varying temperature and salinity . Horizontal dashed lines at y=0 indicate no deviation between observed and calculated pH.

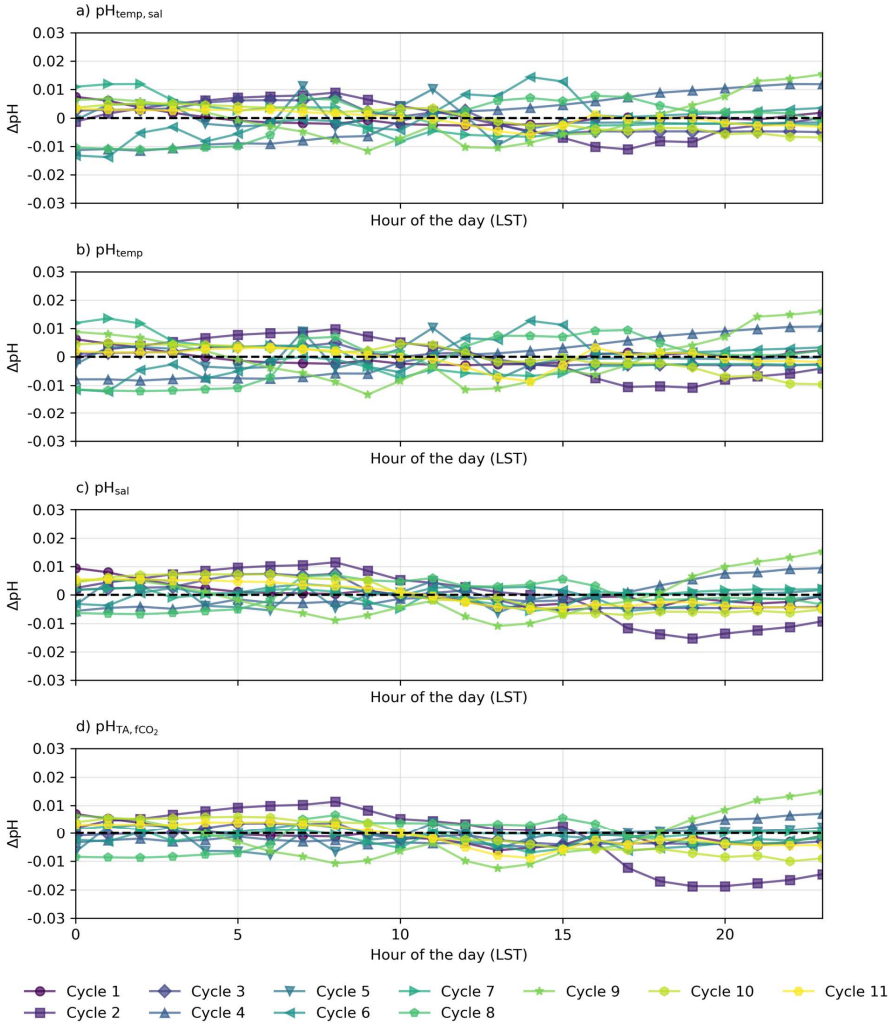

Figure 7. Residual plots for ~~diurnal~~diel cycles in the South Pacific, illustrating the ~~discrepancies~~ differences (ΔpH) between observed pH measured by the optode (pH$_{obs}$) and a) pH calculated from constant TA and DIC with varying temperature and salinity (pH$_{temp,sal}$), b) varying temperature only (pH$_{temp}$), c) varying salinity only (pH$_{sal}$) and d) constant TA and *f*CO$_2$ with varying temperature and salinity . Horizontal dashed lines at y=0 indicate no deviation between observed and calculated pH.

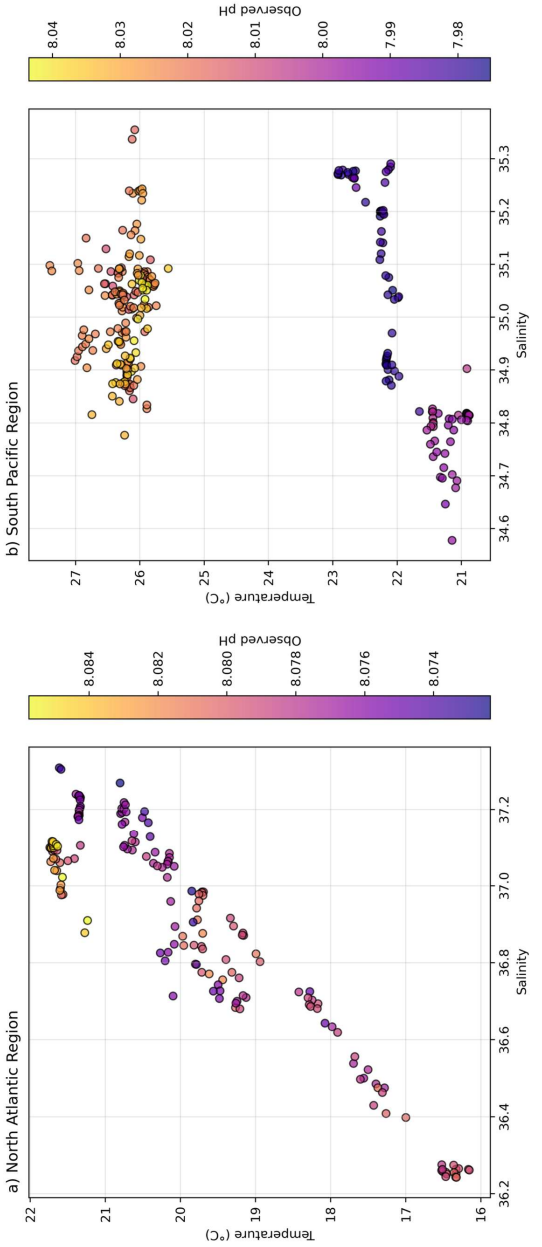

Figure 8. T/S diagram with observed pH for a) the North Atlantic region and b) the South Pacific region.

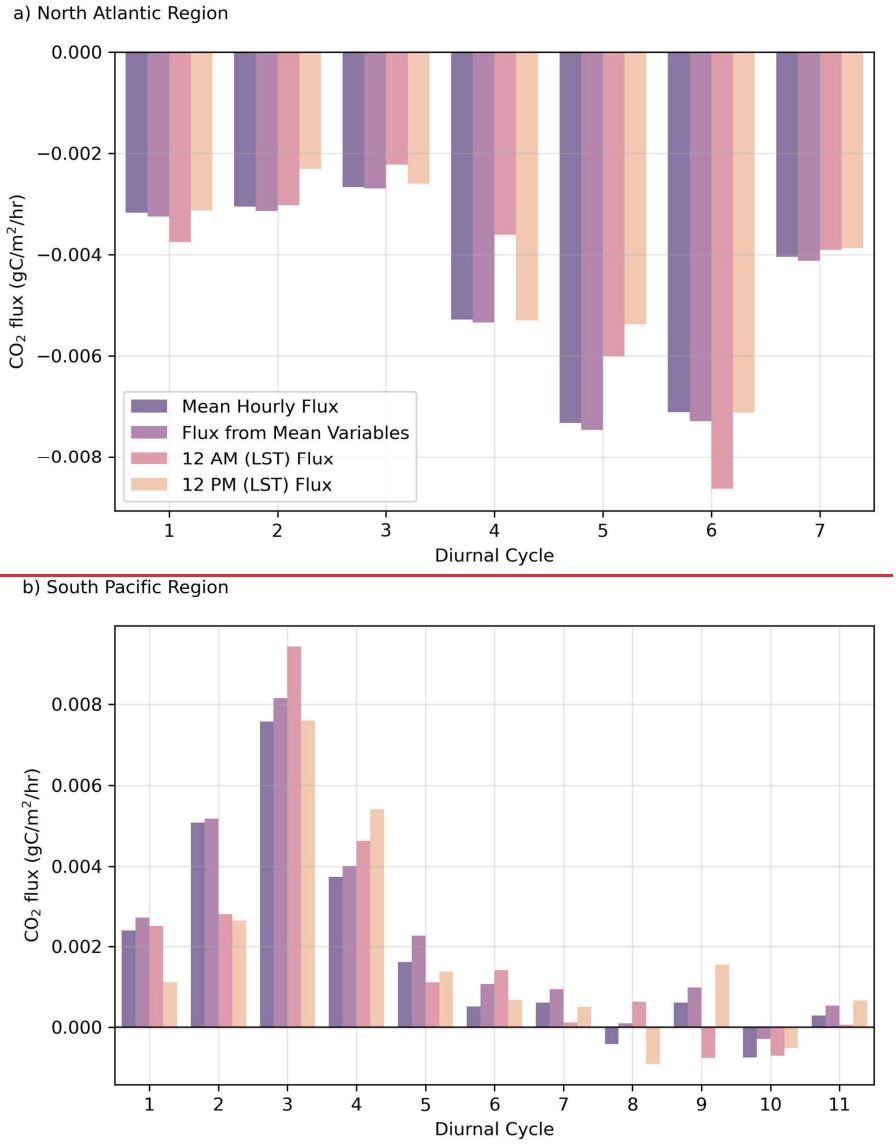

Figure 9. Sensitivity analysis of mean CO_2 flux compared to flux calculated from mean inputs, fluxes for 12 AM (LST) and fluxes for 12 PM (LST). Top panel a) shows cruise SO279 in the North Atlantic while bottom panel b) shows cruise SO289 in the South Pacific.

3 Results and Discussion

We first analyse the effects of temperature and salinity on pH across different ~~diurnal~~diel cycles and regions (Sect. 3.1) using high-resolution pH data enabled by our novel optical measurement system. We examine the pH expected from temperature and salinity variations alone ($pH_{temp,sal}$), disregarding changes in TA or DIC. If pH_{obs} (i.e. corrected underway pH measurements using discrete TA and DIC subsamples) aligns with $pH_{temp,sal}$, it suggests that recent temperature changes, such as day-night cycles, primarily control pH. In this context, "recent" is relative to the air-sea CO_2 equilibration timescale, i.e., temperature change that happened recently enough that its effect on pH has not been modified by subsequent gas exchange. Next, we assess the influence of ~~water mass~~hydrographic variations on pH by considering $pH_{TA,fCO2}$, which accounts for constant fCO_2 instead of DIC alongside constant TA and varying temperature and salinity. Alignment of pH_{obs} with $pH_{TA,fCO2}$ indicates that slower or long-ago processes control pH. For example, an observed change in temperature may be due to spatial variability, with the ship passing through different waters with distinct temperature-salinity properties ~~water masses~~ that have had different temperatures for long enough to reequilibrate with atmospheric CO_2. By leveraging the high-frequency resolution of our measurement system, ~~We~~ we then explore the role of biological activity and its interaction with abiotic factors by looking at the discrepancies between pH_{obs} and both $pH_{temp,sal}$ and $pH_{TA,fCO2}$ (Sect. 3.2). Finally, we distinguish between temporal and spatial variability in our measurements (Sect. 3.3), considering implications for air-sea CO_2 equilibration timescales at fine spatio-temporal scales (Sect. 3.4).

3.1 Influence of temperature and salinity

3.1.1 Basin-scale comparison

The ~~diurnal~~diel cycles of pH observed in the North Atlantic and South Pacific Oceans are significantly influenced by temperature. In the North Atlantic, observed pH stays within ±0.01 of $pH_{temp,sal}$, supporting the role of temperature and salinity in driving pH changes (Fig. 6). However, in the South Pacific, where SNR values for temperature and salinity-driven pH changes remain below 1, observed fluctuations may not exceed measurement noise, making it uncertain whether these variations reflect true environmental signals or instrument variability (Fig. 7; Table S2 in Supplementary Information). ~~In most cycles, observed pH stays within ±0.01 of $pH_{temp,sal}$ thus indicating that temperature and salinity together drive pH changes (Fig. 6 and 7).~~ ~~However, s~~ Despite this, the systematic nature of diel fluctuations—seen across multiple cycles and their correlation with expected temperature-driven trends—suggests they are meaningful rather than random variability.

Salinity alone does not appear to strongly influence pH in any observed cycle. For both ocean basins, pH_{sal} typically remains close to the mean pH of each cycle, rather than impacting the observed pH significantly. This consistency suggests that daily salinity variations do not exert a primary influence on the observed pH (Fig. 4 and 5; Fig. 6c; Fig. 7c; Tables S1 and S2 in Supplementary Information). Thus, the rest of this section focuses on the effect of temperature on the observed pH.

~~On short timescales (minutes and faster), temperature influences pH by affecting the dissociation of carbonic acid (H_2CO_3) into bicarbonate (HCO_3^-) and carbonate (CO_3^{2-}) ions. As temperature~~

Formatted: Font: Not Bold

Formatted: Subscript

~~changes, the dissociation constants of carbonic acid change, which in turn alters the concentrations of these ions and the overall pH of the solution. This dependency shifts the equilibrium of these species with changing temperature and affects pH over short timescales (i.e., seconds to minutes; (Egleston et al., 2010; Stumm & Morgan, 2012). However, the overall response can be lessened by the stabilizing effect of alkalinity, which keeps the pH steady despite temperature changes (Frankignoulle, 1994; Middelburg et al., 2020). The alkalinity of seawater allows the carbonate system and other weak acid-base equilibria to maintain pH by absorbing or releasing protons, which reduces the impact of temperature changes on pH (Dickson & Millero, 1987; Egleston et al., 2010). Typically, the most pronounced temperature fluctuations—highest temperatures during daylight and lowest at night—occur in surface waters. This is due to surface waters' lower thermal inertia and direct exposure to the atmosphere. In contrast, deeper waters have a smaller thermal response because they are insulated from direct atmospheric influence and have a higher heat capacity, which buffers them against rapid temperature changes.~~

In the North Atlantic, the observed variability in pH generally matches the calculated pH_{temp} and $pH_{temp,sal}$, with most cycles' residuals within ±0.01 (Fig. 4 and Fig. 6a and b, Cycles 2, 3, 4, 5 and 6). This agreement suggests that temperature and salinity together explain most of the observed short-term variations. However, some cycles show more pronounced deviations.~~However, some cycles match better than others.~~ Cycle 3 demonstrates a particularly strong ~~a consistent~~ alignment between observed pH and expected $pH_{temp,sal}$ throughout the day~~, with minimal oscillations around the mean~~ (mean residuals ~~<~~ ~~for $pH_{temp,sal}$ of less than~~ -0.001; Fig. 4; Fig. 6a and b)~~. A similar pattern is observed in~~, while Cycle 4 also exhibits minimal variation~~,~~ ~~where pH variations are minimal~~ (residuals ~~range from~~ -0.007 to 0.003 ~~for $pH_{temp,sal}$, with a mean of less than -0.001~~; Fig. 4). ~~In contrast, in Cycle 5, pH_{obs} and $pH_{temp,sal}$ show close agreement throughout the day with residuals close to zero, indicating a stable match despite slight deviations from that day's cycle mean.~~

~~Cycle 6 also displays more pronounced daily fluctuations in pH_{temp} and $pH_{temp,sal}$ with residuals from -0.008 to +0.008 (Fig. 6) but that still closely follow pH_{obs} (within the ±0.01 residuals; Fig. 4).~~ In the South Pacific, pH variability follows a different pattern, While some cycles ~~similar patterns are evident in~~ (eg. Cycles 1, 3, 4, and 6) show a similar agreement between observed pH and $pH_{temp,sal}$ (Fig. 5), overall, the influence of temperature appears weaker than in the North Atlantic. ~~with consistent and minimal fluctuations around the cycle mean (Fig. 5). Cycle 3 in particular shows most stability, with all expected pH values remaining within a narrow range of the observed pH (i.e. mean residuals for $pH_{temp,sal}$ of less than 0.001; Fig. 5; Fig. 7a and b). Similarly, in Cycles 4, 10 and 11, pH_{obs} closely match $pH_{temp,sal}$ across the day, and exhibit minimal residuals (< 0.01; Fig. 5 and 7a and b).~~ The SNR analysis (see Text S1 in Supplementary Information) confirms this, with North Atlantic temperature-driven pH fluctuations exceeding noise (SNR = 1.39 for $pH_{temp,sal}$, 1.20 for pH_{temp}), while all pH variations in the South Pacific remain below SNR = 1 (see Tables S1 and S2 in Supplementary Information). This suggests that in the South Pacific, observed fluctuations may be more influenced by noise than by real temperature-driven variability. However, the persistence of systematic diel fluctuations suggests that meaningful signals are still present.

Formatted: Subscript

Formatted: Not Superscript/ Subscript

Formatted: Subscript

Formatted: Subscript

The physical oceanographic context of each basin likely contributes to these differences. In the North Atlantic, significant mixing due to ocean currents, eddies, and upwelling introduces substantial variability in temperature, salinity, and pH across different waters with distinct temperature-salinity properties (Fig. 6a and b; see Fig. S6 in Supplementary Information). The Gulf Stream and North Atlantic Drift contribute to this complexity, which may help maintain stronger temperature-driven pH changes by continuously exposing surface waters to variable thermal forcing (Liu & Tanhua, 2021). In contrast, the South Pacific exhibits more predictable hydrographic dynamics, driven largely by advection and mixing within large-scale gyres and trade wind systems (Vallis, 2017). This results in a more stable and homogeneous water column, where observed pH fluctuations remain closer to the measurement uncertainty (Fig. 7).

3.1.2 Diel pH variability

Beyond the basin-scale differences, a key feature of the observed pH cycles is the variability between daytime and nighttime conditions. In both basins, temperature changes between day and night are expected to drive corresponding pH shifts due to the temperature dependence of the carbonate system.

In the North Atlantic, observed pH generally follows expected temperature-driven changes, with pH_{temp} and $pH_{temp,sal}$ showing higher values at night and lower values during the day due to the inverse relationship between temperature and pH (Fig. 4, Fig. 6). For example, in Cycles 3 and 6, the residuals between observed and expected pH remain small throughout the day, reinforcing the dominance of temperature as a control mechanism. However, in some cycles (e.g., Cycle 1), nighttime pH remains elevated beyond what would be expected from temperature alone, suggesting the influence of additional processes such as biological activity or air-sea CO_2 exchange.

In the South Pacific, similar diel patterns are present but exhibit greater variability across cycles. Some cycles (e.g., Cycle 8) show clear daytime decreases and nighttime increases in pH, consistent with temperature-driven changes (Fig. 5). However, in other cases (e.g., Cycle 9), observed pH departs from the expected diel pattern, indicating that other factors may be influencing short-term variability.

The persistence of nighttime pH anomalies in both basins raises questions about equilibration timescales. While temperature-driven changes in pH and fCO_2 occur rapidly in response to solubility and speciation shifts, CO_2 equilibration between the atmosphere and ocean occurs over much longer timescales (weeks to months; (Jones et al., 2014)). This means that pH adjustments due to temperature occur almost instantly, but whether they persist over a full diel cycle depends on the history of the hydrographic properties. If waters have recently equilibrated with the atmosphere, its pH should closely follow $pH_{temp,sal}$. However, if these waters have undergone rapid temperature shifts without sufficient time for equilibration, observed pH may diverge from temperature-based expectations. This highlights the interplay between rapid thermodynamic effects and longer equilibration processes, particularly in regions like the North Atlantic, where mixing introduces additional complexity.

Ultimately, our observations suggest that while temperature is a dominant driver of diel pH changes, the extent to which these changes persist overnight depends on the physical

Formatted: Heading-Secondary
Formatted: Subscript
Formatted: Subscript
Formatted: Font: Not Bold
Formatted: Font: Not Bold, Italic
Formatted: Font: Not Bold
Formatted: Subscript
Formatted: Font: Not Bold
Formatted: Subscript
Formatted: Font: Not Bold
Formatted: Font: Not Bold
Formatted: Subscript

characteristics of the surface waters and their equilibration history. In the North Atlantic, where mixing is more dynamic, the system appears to re-equilibrate more readily, whereas in the South Pacific, longer equilibration timescales may contribute to greater deviations from expected pH patterns.

~~However, notable discrepancies occur in pH observations versus calculated pH_{temp} and $pH_{temp,sal}$ in the North Atlantic. Specifically, in Cycle 1, while pH_{obs} remains relatively stable, there are significant daily fluctuations in pH_{temp} and $pH_{temp,sal}$, with residuals ranging from -0.023 to 0.029 and a mean of less than -0.001 (Fig. 4; Fig. 6a, b, and c). Cycles 5 and 7 also show discrepancies: although pH_{obs} generally matches the cruise mean across all cycles, $pH_{temp,sal}$ exhibits greater deviations, indicating that some other process has eliminated the temperature signal in the observed pH (Fig. 4; Fig. 6a and b). In the South Pacific, similar patterns emerge. Cycle 5 shows significant hourly fluctuations in pH_{obs}, which closely track the deviations in pH_{temp} and $pH_{temp,sal}$, markedly diverging from the more stable pH_{sal} (Fig. 5; Fig. 7a and b). Additionally, in Cycle 2, the initial excess and subsequent shortfall in pH_{temp} and $pH_{temp,sal}$, with residuals from -0.011 to 0.008, suggest a comparable moderated effect by solar heating (Fig. 4). This pattern is consistent with observations in the North Atlantic. This overriding influence, likely due to solar heating, impacts the diurnaldiel pH fluctuation patterns, particularly in cycles where pH_{temp} and $pH_{temp,sal}$ start higher and decrease throughout the day.~~

~~While changes in pH and fCO_2 due to temperature change occur virtually instantaneously (i.e., seconds to minutes), CO_2 equilibration between the atmosphere and the ocean is considerably slower (i.e., weeks to months; Jones et al. (2014). This means that the timescale of temperature change significantly influences how a water masses' pH adjusts to temperature changes (Takahashi et al., 2009). For instance, when a water mass cools during the night, it quickly alters pH and causes CO_2 undersaturation due to increased solubility, so observed pH would agree with pH_{temp} (Feely et al., 2008). However, as the ship travels through different water masses that vary in temperature, but are each in equilibrium with the atmosphere, observed pH may not align with pH_{temp} or $pH_{temp,sal}$ calculated based on temperature shifts alone. This raises an issue regarding the timescales of temperature change in relation to chemical equilibration, as it is uncertain whether these changes provide the system enough time for fCO_2 (and DIC) to shift and maintain equilibrium with the atmosphere, or if they happen more rapidly, such that disequilibrium remains.~~

~~In the North Atlantic, significant mixing due to ocean currents, eddies, and upwelling introduces substantial variability in temperature, salinity, and pH across different water masses (Fig. 6a and b). This variability is further influenced by the Gulf Stream and North Atlantic Drift, which create complex structures of distinct water masses (Liu & Tanhua, 2021). These dynamic conditions adjust the rate of CO_2 absorption or release, impacting the timescale over which ocean-atmosphere equilibrium is achieved. But in this ocean basin, $pH_{TA,fCO2}$ (i.e. proxy for gas-exchange equilibrium) follows pH_{obs} very closely, indicating that temperature changes have been sufficient for the system to reach re-equilibration. This is true both for individual cycles' diurnaldiel distributions (Fig. 4), and when comparing the cycles' residuals together, which are virtually zero (Fig. 6d), even during temperature gradient crossings (Fig. S4).~~

~~In contrast, the South Pacific displays more predictable water mass dynamics primarily driven by physical processes like mixing and advection, which introduce water masses with consistent temperatures, salinities, and pH, resulting in a more homogeneous water column. This stability is influenced by large-scale gyres and trade winds, contributing to the uniformity of surface waters (Vallis, 2017). This is reflected by the consistent pH_{obs}. Residuals are further from zero although most cycles fall within ±0.01, indicating a lesser degree of re-equilibration (Fig. 7).~~

~~Thus, this implies that, in both ocean basins, gas exchange plays a significant role in stabilizing pH for all cycles by re-equilibrating with atmospheric CO_2 despite temperature fluctuations – although it likely does more so in the North Atlantic than in the South Pacific. To first order, this also suggests that the temperature change happened long enough ago for re-equilibration. However, the rates of gas exchange in the North Atlantic and South Pacific are from 3 to 6 months and 3 to 4 months, respectively (Jones et al., 2014). Thus, the consistency between $pH_{TA,fCO2}$ and pH_{obs} likely represents the crossings of water masses that are in equilibrium with the atmosphere and that equilibrated a long time ago (i.e., weeks to months) with different TA, DIC, and temperature baselines. Thus, the observed temperature changes as the ship traverses different water masses are likely attributable to spatial variations rather than an immediate response to recent temperature shifts. However, some pH cycles observed do not fully conform to these patterns, suggesting that other factors could be influencing the pH beyond the effects of temperature and gas exchange alone.~~

~~Ultimately, although we observe temperature-induced variations throughout each diurnal~~diel ~~cycle, when comparing all cycles' pH_{obs}, pH_{temp} and $pH_{temp,sal}$ within both ocean basins, residuals are well within ±0.02 (Fig. 6a and b and Fig. 7a and b). Thus, despite observed 24-hour fluctuations, pH remains relatively stable with respect to temperature variations across both ocean basins. This stability implies that even though there are short-term fluctuations in pH due to temperature changes, overall the pH stays relatively consistent, and thus a stable ocean-atmosphere CO_2 equilibrium.~~

3.2 Influence of biological activity

While temperature and salinity effects on pH have been addressed in Sect. 3.1, deviations from expected patterns may be shaped by biological processes. The process of photosynthesis during daylight consumes CO_2, leading to a rise in pH, whereas respiration and decomposition at night, which release CO_2, lower pH (Falkowski, 1994; Falkowski & Raven, 2013). The balance between photosynthesis and respiration hence affects pH, and should result in a ~~diurnal~~diel pH cycle. However, biological signals in the open ocean are often weaker than in coastal or upwelling regions due to lower phytoplankton biomass and primary production rates (Behrenfeld & Falkowski, 1997; Johnson et al., 2010). As a result, strong diel biological pH signals are not typically expected in oligotrophic oceanic waters. These biological processes can also influence the rate at which CO_2 equilibrates between the ocean and atmosphere. For instance, intense photosynthetic activity during daylight hours can rapidly deplete seawater pCO_2 in surface waters, potentially accelerating seawater CO_2 uptake from the atmosphere. Conversely, nighttime respiration can increase pCO_2, slowing the outgassing process and thus extending the equilibration timescale. However, given an equilibration timescale of months, these day and night changes likely get averaged out over longer periods, resulting in an overall steady-state CO_2 flux and pH when observed over longer temporal scales.

These biological processes are particularly evident in some cycles from the North Atlantic where the expected $pH_{temp,sal}$ changes due to temperature and salinity do not align with the observed data, but do follow the distribution expected from biological activity (Fig. 4).). However, the strength of these pH variations should be interpreted with caution, as biological activity in open-ocean regions tends to be relatively low (Longhurst, 2010). The North Atlantic subtropical gyre, for instance, has low rates of primary productivity (Baines et al., 1994; Tilstone et al., 2003), which suggests that biological-driven pH variations would be relatively small. This is especially evident for Cycle 1, which shows an increase in pH during daylight hours and a decrease in pH during night hours, with a peak in pH in late afternoon and the lowest pH occurring in the early morning before sunrise (Fig. 4). Other cycles likely reflect the combined impact of biological processes and temperature effects, as the observed pH does not fully align with the distribution expected from any of temperature, salinity or biological activity (Fig. 4 and 6). ~~This is also evidentI in~~ In the South Pacific Ocean, ~~where~~ some cycles show significant variability within pH_{obs} that are not mirrored by the expected $pH_{temp,sal}$ changes (Fig. 5, Cycles 2, 8). For example, Cycle 2 exhibits significant deviations in pH with higher observed values in the morning and a drop in the afternoon~~, indicating biological influence~~ (Fig. 5). Although this suggests a potential biological influence, the SNR values remain below 1 across all expected pH estimates, making it unclear whether the observed fluctuations are truly driven by biological activity or simply fall within the instrument's noise threshold (Table S2 in Supplementary Information).

The interplay between photosynthesis during the day and respiration at night, with possible contributions of other biological processes, may be behind the more pronounced peaks and troughs of Cycles 2 and 9 (Fig. 6; Duarte and Agusti (1998). Nitrogen fixation consumes hydrogen ions, increasing pH, whereas denitrification releases hydrogen ions, thereby decreasing pH (Richardson, 2000; Zehr & Kudela, 2011). However, without nutrient and oxygen data, we cannot directly assess whether these processes also impacted the observed pH.

Although biological activity likely accounts for some variability, not all cycles exhibit the same residual, presumably biotic pattern of variation (Fig. 4 and 5). This aligns with expectations, as phytoplankton biomass and primary productivity in open-ocean regions can be highly variable, and biological impacts on carbonate chemistry are typically more pronounced in coastal or upwelling systems (Duarte & Agusti, 1998; Williams & Follows, 2003). Moreover, the SNR results indicate that in the North Atlantic, temperature-driven processes dominate short-term pH variability, while the contribution of biological activity remains unclear due to overlapping influences (see Table S1 in Supplementary Information). In the South Pacific, where all signals fall below the noise threshold (SNR < 1; Table S2 in Supplementary Information), the observed pH fluctuations may be driven by measurement uncertainty rather than a clear biological or temperature-driven signal.

This variability further complicates assessments of air-sea CO_2 equilibration, as localized biological conditions may transiently alter CO_2 dynamics, influencing the timescale for reaching equilibrium. This is more obvious in the South Pacific, where some cycles display more pronounced night-time stability (Fig. 5, Cycles 3, 6, 7 and 11), while others have noticeable day-time fluctuations that could align with photosynthetic activity, which typically increase during daylight hours (Fig. 5, Cycle 8; (Duarte & Agusti, 1998; Raven & Johnston, 1991). Cycle 8 in

the South Pacific shows a peak in observed pH around midday, likely due to increased photosynthesis, followed by a decrease in the evening (Fig. 5). Other cycles do not show this pattern as clearly (i.e., they even show a decrease of pH during the day), suggesting that, for some cycles, respiration may dominate over photosynthesis also during daytime (Fig. 5). For example, Cycle 9 displays significant variations in pH throughout the day, with notable decreases during daylight hours (Fig. 5). Additionally, as some cycles appear to conform to temperature-based pH expectations, the only minor deviations observed suggest biological activity to be minor or represent a balanced biological system where photosynthesis and respiration are in near-equilibrium (Fig. 5, Cycles 3 and 6).

Despite the strong impact of both abiotic and biotic factors on pH, some cycles exhibit fine-scale trends that cannot be solely attributed to temperature fluctuations or biological activity. The fine-scale trends observed, especially in Cycles 1 and 7 (Fig. 4), exceed what can be attributed to temperature-induced changes alone and cannot be explained by biological activity, given the atypically high carbon fixation rates required to explain the pH offsets (Basu & Mackey, 2018; Wang et al., 2023). Indeed, the required biological carbon fixation would need to exceed 687 mg C m^{-3} day to explain the offset (Text S~~7~~2). Typical rates in open ocean waters are much lower, generally ranging from 50 to 150 mg C m^3 day^{-1} in nutrient-poor regions and can reach up to 1000 C m^{-3} day^{-1} in upwelling zones during phytoplankton blooms, which is not the case here (Basu & Mackey, 2018; Wang et al., 2023).

Comparing the impact of biological activity based on the offsets between pH_{temp} and pH_{obs} with chlorophyll-a fluorescence data also shows no clear pattern (Fig. S~~4~~2 and S~~5~~3). This is expected as fluorescence does not necessarily reflect instantaneous photosynthetic activity. Instead, fluorescence primarily indicates the presence and abundance of phytoplankton. Therefore, while fluorescence can provide insights into the overall biomass of phytoplankton, it does not directly correlate with photosynthesis and respiration. The absence of a clear correlation between fluorescence and the daily pH cycle, with some cycles even showing a decrease in pH during daytime, confirms that the influence of waters with distinct temperature-salinity properties~~different water masses~~ is important in shaping the local high-resolution pH profiles.

3.3 Variability and stability in spatio-temporal pH patterns

~~The North Atlantic is characterized by complex interactions among water masses, leading to higher turbulence and susceptibility to rapid and significant changes in water mass properties and circulation patterns, influenced by both past and present climatic conditions (Lynch-Stieglitz, 2017; Gebbie, 2014). This complexity is partly due to the Atlantic Meridional Overturning Circulation (AMOC), which is sensitive to various climate perturbations and has historically undergone significant reorganizations, especially during climatic transitions such as the Last Glacial Maximum (Curry and Oppo, 2005; Duplessy et al., 1988).~~ As examined in Sect. 3.1, considerable spatial variability is observed in the North Atlantic (Fig. 8 and Fig. S~~6~~8), and this heterogeneity introduces complexity in deciphering the relative contributions of abiotic and biotic factors to pH fluctuations (Gruber & Sarmiento, 2002). Residual plots for the North Atlantic suggest that the observed discrepancies between pH_{obs} and both pH_{temp} and $pH_{temp,sal}$ are insignificant, indicating that variability in surface water ~~mass~~ characteristics—which include but are not limited solely to temperature and salinity—do not dominate the observed pH variability (Fig. 6 and 8; (Dumousseaud et al., 2010)~~)~~. The SNR results further confirm that temperature-

driven pH fluctuations are real signals in this region (SNR > 1; Table S1 in Supplementary Information), supporting their role as key drivers of diel pH variability. Therefore, the hourly fluctuations in pH_{obs} and the observed discrepancies between pH_{obs} and $pH_{temp/sal}$ across various cycles in this ocean basin may not be attributed to pronounced spatial variability (Fig. 4). The T/S diagram also demonstrates this spatial variability, showing a wide range of pH values correlated with differing salinity and temperature profiles across waters with distinct temperature-salinity properties ~~various water masses~~ (Fig. 8), reinforcing that spatial dynamics do not significantly influence pH variation in this region. This is also supported by the relative stability observed in Cycle 4, where the ship's consistent positioning (i.e. on station) highlights the role of temporal variability rather than spatial variability (Fig. S64). Although water could still be moving spatially around the ship, the variability could be due to some degree to different waters ~~masses~~ rather than being limited to true in-situ temporal variability.

In contrast, the South Pacific cruise predominantly exhibits a stable transit through more homogeneous surface waters as no SST gradient is observed, although it is not entirely free from disruptions (Fig. 8 and Fig. S75; Qu and Lindstrom (2004). This suggests a ~~minor~~ limited role of interactions between diverse surface waters ~~masses~~. Despite the hourly fluctuations observed, all ~~diurnal~~diel cycles in the South Pacific tend to cluster closely around the mean pH for their respective 24-hour periods, reflecting substantial stability within each cycle but considerable variability across different days, particularly evident among consecutive cycles (Fig. 5). This underscores a clear temporal delineation of ~~diurnal~~diel cycles influenced by DIC changes (Fig. 5). However, the SNR results indicate that all expected pH fluctuations in this region remain below the uncertainty threshold (SNR < 1; Table S2 in Supplementary Information), making it difficult to determine whether observed fluctuations reflect true environmental variability or are primarily within the measurement uncertainty.

3.4 Implications for air-sea CO_2 fluxes

Our findings indicate that while temperature and salinity predominantly govern ~~diurnal~~diel pH fluctuations, additional variability arises from surface water ~~mass~~ dynamics and biological activity. Temperature rapidly affects pH, but the slower rate of CO_2 equilibration with the atmosphere moderates its impact on air-sea CO_2 fluxes. Although biological processes markedly influence daily pH cycles, they do not fully account for the observed variability, especially in cases where unusually high carbon fixation rates would be required to explain observed pH (Sect. 3.2). Notably, the North Atlantic acted as a net sink of CO_2, whereas the South Pacific was a net source to the atmosphere during the study period.

CO_2 fluxes were calculated for each complete ~~diurnal~~diel cycle (Fig. 9). The flux calculations were performed by computing the mean flux for each cycle from daily mean inputs (wind speed, temperature, salinity, and pCO_2) and specifically for the hours 12 AM and 12 PM (LST) to examine temporal variations within each cycle (Fig. 9). Despite different methods of calculation, the CO_2 fluxes remained relatively consistent, indicating that the variations in pH and thus CO_2 flux do not significantly affect the air-sea CO_2 exchange in either basin.

This consistent result shows that, despite the processes influencing pH in these two ocean basins during the study period, air-sea CO_2 exchange over longer timescales (e.g., months) can dampen short-term pH variability, resulting in relatively low variability across short spatiotemporal scales

Formatted: Subscript

Formatted: Subscript

(kilometers/days).~~This consistent result shows that despite the processes influencing pH in these two ocean basins during the study period, the surface ocean's interaction with atmospheric CO_2 over longer timescales (eg. months) can minimize the effect on pH, leading to relatively low variability on short spatiotemporal scales (kilometers/days).~~

4. Conclusions

High-resolution pH data enabled by our novel optical measurement system ~~is crucial~~provides valuable insights ~~for understanding the subtle yet important variations in~~ into the complex and variable nature of ~~ocean~~ surface ~~water~~ ocean pH ~~across different regions~~. Our observations in the North Atlantic and South Pacific show that pH fluctuates on diel and hourly timescales, with variations driven not only by temperature but also by the interplay between waters with distinct temperature-salinity properties and biological activity. These factors do not operate in isolation, making it difficult to attribute pH changes to a single dominant driver.~~Diurnal~~Diel ~~cycles and hourly fluctuations in pH, with varying magnitudes, can be observed in both the North Atlantic and South Pacific basins. Variability in pH is influenced not only by temperature but also by interactions between various water masses and biological activity. These factors together drive observed pH fluctuations, often diverging from predictions based solely on temperature. However, although the processes responsible for these pH variations are well-understood, high-resolution data highlight the challenge of identifying a dominant factor at the fine-scale due to their complex interplay.~~

~~In both the North Atlantic and South Pacific, the close correlation between $pH_{TA,fCO2}$ and observed pH across diurnal~~diel ~~cycles suggests a significant role of gas exchange in stabilising pH despite temperature fluctuations. The temperature changes must therefore have happened more slowly than the air-sea CO_2 equilibration timescales for these ocean basins. The observed, relatively constant pH is likely due to the ship passing through different water masses that had already equilibrated with the atmosphere.~~

Although the processes governing pH variability are well-understood, our high-frequency measurements demonstrate the challenge of disentangling their contributions at fine spatial and temporal scales. This underscores the importance of continuous, high-frequency measurements, which reveal the heterogeneity in surface pH that lower-resolution datasets might miss. In both basins, the close correlation between pH_{TA,fCO_2} and observed pH across diel cycles suggests that air-sea CO_2 exchange plays a key role in stabilizing pH despite temperature fluctuations. The observed pH stability implies that the ship primarily encountered waters that had already equilibrated with atmospheric CO_2, reinforcing the idea that temperature-driven pH changes alone are not always sufficient to explain variability in surface ocean carbonate chemistry.

~~Thus, despite short-term fluctuations in pH, there were no major changes in ocean-atmosphere CO_2 disequilibrium, indicating that, for the regions and time periods studied here, broader ocean-basin scale analyses based on lower resolution datasets would still be able to capture the necessary variability in surface ocean CO_2 chemistry for accurate global CO_2 cycle assessments.~~

While our results indicate that fine-scale variability in these regions was relatively subtle—and may not significantly impact large-scale assessments—this insight could only be gained through high-resolution observations. This approach not only reveals the complexity of pH regulation but

Commented [LD6]: Needs to mention timescale and space vs time issues for air sea gas exchange and co2 eq

Commented [LD7R6]: Thus, in regions like the North Atlantic, where deep water formation and upwelling might be prevalent, CO_2 equilibration times could be extended due to the constant influx of deeper, CO_2-rich waters. Conversely, in the South Pacific, especially in areas with less intense upwelling and warmer temperatures, CO_2 equilibration could occur more rapidly.

Formatted: Subscript

Formatted: Subscript

Formatted: Subscript

also provides valuable insight into the fine-scale physical and biological interactions that shape surface ocean chemistry. Importantly, although lower-resolution datasets may be sufficient for capturing broad-scale patterns in surface ocean CO_2 chemistry, our findings highlight the critical role of high-frequency measurements in refining regional understanding and improving predictive models of ocean acidification and air-sea gas exchange.

Formatted: Subscript

Data availability. The hydrographic and biogeochemical data presented here, together with the processing code ~~will be~~ is freely available online at https://github.com/louisedelaigue/NA-SP-HIGH-RES-PH. ~~by the time of publication.~~

Supplement. The supplement related to this article is available online.

Author contributions. LD and MPH conceptualized the project. CG, AM, LQ, EPA, LD, MPH and YO curated the data. LD, MPH and GJR performed the investigation. LD conceptualized the methodology, used the necessary software, visualized the data and prepared the original draft of the paper. LD, GJR, MPH, YO and ~~and~~ CG reviewed and edited the paper.

Competing interests. The contact author has declared that neither they nor their co-authors have any competing interests.

Disclaimer. Publisher's note: Copernicus Publications remains neutral with regard to jurisdictional claims in published maps and institutional affiliations.

Acknowledgements. We are grateful to the officers and crew of the R/V *Sonne* and technical support from GEOMAR for their support and assistance, and the opportunity to join cruises SO279 and SO289. Special acknowledgment goes to Paul Battermann who greatly assisted in the sampling aboard the FS Sonne during SO289. Funding for cruise SO289 came from the BMBF (grant 03G0289NA) to EPA. We thank Karel Bakker and Sharyn Ossebaar for their help in the lab – this work would not be possible without them. LD also wishes to thank Sorbonne Université and the Institut de la mer de Villefranche (France), in particular the OMTAB team, for hosting her during the later stage of this research project, as well as Jean-Pierre Gattuso, Pierrick Lemasson and Elsa Simon for the many brainstorming sessions. Figure 2 schematic made by cartographic design - faculty of Geosciences - Utrecht University.

References

Achterberg, E. P., Steiner, Z., & Galley, C. G. (2022). South Pacific GEOTRACES Cruise No. SO289, 18 February 2022–08 April 2022, Valparaiso (Chile)–Noumea (New Caledonia), GEOTRACES GP21.

Baines, S. B., Pace, M. L., & Karl, D. M. (1994). Why does the relationship between sinking flux and planktonic primary production differ between lakes and oceans? *Limnology and Oceanography*, *39*(2), 213-226.

Basu, S., & Mackey, K. R. M. (2018). Phytoplankton as Key Mediators of the Biological Carbon Pump: Their Responses to a Changing Climate. *Sustainability*, *10*(3), 869. https://www.mdpi.com/2071-1050/10/3/869

Beck, A., Borchert, E., Delaigue, L., Deng, F., Gueroun, S., Hamm, T., Jacob, O., Kaandorp, M., Kokuhennadige, H., & Kossel, E. (2021). NAPTRAM-Plastiktransportmechanismen, Senken und Interaktionen mit Biota im Nordatlantik/NAPTRAM-North Atlantic plastic

transport mechanisms, sinks, and interactions with biota, Cruise No. SO279, Emden (Germany)–Emden (Germany), 04.12. 2020–05.01. 2021.

Behrenfeld, M. J., & Falkowski, P. G. (1997). Photosynthetic rates derived from satellite-based chlorophyll concentration. *Limnology and Oceanography*, *42*(1), 1-20.

Caldeira, K., & Wickett, M. E. (2005). Ocean model predictions of chemistry changes from carbon dioxide emissions to the atmosphere and ocean. *Journal of Geophysical Research: Oceans*, *110*(C9).

Chavez, F. P., Sevadjian, J., Wahl, C., Friederich, J., & Friederich, G. E. (2018). Measurements of pCO2 and pH from an autonomous surface vehicle in a coastal upwelling system. *Deep Sea Research Part II: Topical Studies in Oceanography*, *151*, 137-146. https://doi.org/https://doi.org/10.1016/j.dsr2.2017.01.001

Cornwall, C. E., Hepburn, C. D., McGraw, C. M., Currie, K. I., Pilditch, C. A., Hunter, K. A., Boyd, P. W., & Hurd, C. L. (2013). Diurnal fluctuations in seawater pH influence the response of a calcifying macroalga to ocean acidification. *Proceedings of the Royal Society B: Biological Sciences*, *280*(1772), 20132201. https://doi.org/doi:10.1098/rspb.2013.2201

Couldrey, M. P., Oliver, K. I., Yool, A., Halloran, P. R., & Achterberg, E. P. (2016). On which timescales do gas transfer velocities control North Atlantic CO2 flux variability? *Global Biogeochemical Cycles*, *30*(5), 787-802.

Cryer, S., Carvalho, F., Wood, T., Strong, J. A., Brown, P., Loucaides, S., Young, A., Sanders, R., & Evans, C. (2020). Evaluating the Sensor-Equipped Autonomous Surface Vehicle C-Worker 4 as a Tool for Identifying Coastal Ocean Acidification and Changes in Carbonate Chemistry. *Journal of Marine Science and Engineering*, *8*(11), 939. https://www.mdpi.com/2077-1312/8/11/939

Delaigue, L., Ourradi, Y., Bakker, K., Battermann, P., Galley, C., & Humphreys, M. P. (2023a). *Discrete underway surface seawater dissolved inorganic carbon and total alkalinity for R/V Sonne cruise SO289* (Version V2) NIOZ. https://doi.org/doi:10.25850/nioz/7b.b.vf

Delaigue, L., Ourradi, Y., Bakker, K., Battermann, P., Galley, C., & Humphreys, M. P. (2023b). *Underway surface seawater high-resolution pH time series for R/V Sonne cruise SO289* (Version V2) NIOZ. https://doi.org/doi:10.25850/nioz/7b.b.uf

Delaigue, L., Ourradi, Y., Ossebar, S., Battermann, P., Galley, C., & Humphreys, M. P. (2023). *CTD seawater dissolved inorganic carbon and total alkalinity for R/V Sonne cruise SO289* (Version V6) NIOZ. https://doi.org/doi:10.25850/nioz/7b.b.tf

Delaigue, L., van Ooijen, J., & Humphreys, M. P. (2021a). *CTD seawater dissolved inorganic carbon, total alkalinity and nutrients for R/V Sonne cruise SO279* (Version V2) NIOZ. https://doi.org/doi:10.25850/nioz/7b.b.kc

Delaigue, L., van Ooijen, J., & Humphreys, M. P. (2021b). *Discrete underway surface seawater dissolved inorganic carbon, total alkalinity and nutrients for R/V Sonne cruise SO279* (Version V2) NIOZ. https://doi.org/doi:10.25850/nioz/7b.b.lc

Delaigue, L., van Ooijen, J., & Humphreys, M. P. (2021c). *Underway surface seawater high-resolution pH time series for R/V Sonne cruise SO279* (Version V2) NIOZ. https://doi.org/doi:10.25850/nioz/7b.b.mc

DeVries, T. (2022). The Ocean Carbon Cycle. *Annual Review of Environment and Resources*, *47*(1), 317-341. https://doi.org/10.1146/annurev-environ-120920-111307

Dickson, A., & Millero, F. J. (1987). A comparison of the equilibrium constants for the dissociation of carbonic acid in seawater media. *Deep Sea Research Part A. Oceanographic Research Papers*, *34*(10), 1733-1743.

Dickson, A. G. (1990). Standard potential of the reaction: AgCl(s) + 12H2(g) = Ag(s) + HCl(aq), and and the standard acidity constant of the ion HSO4− in synthetic sea water from 273.15 to 318.15 K. *The Journal of Chemical Thermodynamics*, *22*(2), 113-127. https://doi.org/https://doi.org/10.1016/0021-9614(90)90074-Z

Dickson, A. G., & Riley, J. P. (1979). The estimation of acid dissociation constants in sea-water media from potentiometric titrations with strong base. II. The dissociation of phosphoric acid. *Marine Chemistry*, *7*(2), 101-109. https://doi.org/https://doi.org/10.1016/0304-4203(79)90002-1

Dickson, A. G., Sabine, C. L., & Christian, J. R. (2007). *Guide to best practices for ocean CO2 measurements*. North Pacific Marine Science Organization.

Doney, S. C., Busch, D. S., Cooley, S. R., & Kroeker, K. J. (2020). The Impacts of Ocean Acidification on Marine Ecosystems and Reliant Human Communities. *Annual Review of Environment and Resources*, *45*(Volume 45, 2020), 83-112. https://doi.org/https://doi.org/10.1146/annurev-environ-012320-083019

Duarte, C. M., & Agusti, S. (1998). The CO2 balance of unproductive aquatic ecosystems. *Science*, *281*(5374), 234-236. https://doi.org/10.1126/science.281.5374.234

Dumousseaud, C., Achterberg, E. P., Tyrrell, T., Charalampopoulou, A., Schuster, U., Hartman, M., & Hydes, D. J. (2010). Contrasting effects of temperature and winter mixing on the seasonal and inter-annual variability of the carbonate system in the Northeast Atlantic Ocean. *Biogeosciences*, *7*(5), 1481-1492. https://doi.org/10.5194/bg-7-1481-2010

Egea, L. G., Jiménez-Ramos, R., Hernández, I., Bouma, T. J., & Brun, F. G. (2018). Effects of ocean acidification and hydrodynamic conditions on carbon metabolism and dissolved organic carbon (DOC) fluxes in seagrass populations. *PLOS ONE*, *13*(2), e0192402. https://doi.org/10.1371/journal.pone.0192402

Egilsdottir, H., Noisette, F., Noël, L. M. L. J., Olafsson, J., & Martin, S. (2013). Effects of pCO2 on physiology and skeletal mineralogy in a tidal pool coralline alga Corallina elongata. *Marine Biology*, *160*(8), 2103-2112. https://doi.org/10.1007/s00227-012-2090-7

Egleston, E. S., Sabine, C. L., & Morel, F. M. (2010). Revelle revisited: Buffer factors that quantify the response of ocean chemistry to changes in DIC and alkalinity. *Global Biogeochemical Cycles*, *24*(1).

Emerson, S., & Hedges, J. (2008). *Chemical oceanography and the marine carbon cycle*. Cambridge University Press.

Faassen, K. A. P., Nguyen, L. N. T., Broekema, E. R., Kers, B. A. M., Mammarella, I., Vesala, T., Pickers, P. A., Manning, A. C., Vilà-Guerau de Arellano, J., Meijer, H. A. J., Peters, W., & Luijkx, I. T. (2023). Diurnal variability of atmospheric O2, CO2, and their exchange ratio above a boreal forest in southern Finland. *Atmos. Chem. Phys.*, *23*(2), 851-876. https://doi.org/10.5194/acp-23-851-2023

Falkowski, P. G. (1994). The role of phytoplankton photosynthesis in global biogeochemical cycles. *Photosynthesis Research*, *39*(3), 235-258. https://doi.org/10.1007/BF00014586

Falkowski, P. G., & Raven, J. A. (2013). *Aquatic photosynthesis*. Princeton University Press.

Fay, A. R., Gregor, L., Landschützer, P., McKinley, G. A., Gruber, N., Gehlen, M., Iida, Y., Laruelle, G. G., Rödenbeck, C., Roobaert, A., & Zeng, J. (2021). SeaFlux: harmonization

Formatted: French (France)

Formatted: French (France)

Formatted: French (France)

Field Code Changed

of air–sea CO2 fluxes from surface pCO2 data products using a standardized approach. *Earth Syst. Sci. Data*, *13*(10), 4693-4710. https://doi.org/10.5194/essd-13-4693-2021

Fietzek, P., Fiedler, B., Steinhoff, T., & Körtzinger, A. (2014). In situ quality assessment of a novel underwater p CO 2 sensor based on membrane equilibration and NDIR spectrometry. *Journal of Atmospheric and Oceanic Technology*, *31*(1), 181-196.

Figuerola, B., Hancock, A. M., Bax, N., Cummings, V. J., Downey, R., Griffiths, H. J., Smith, J., & Stark, J. S. (2021). A Review and Meta-Analysis of Potential Impacts of Ocean Acidification on Marine Calcifiers From the Southern Ocean [Review]. *Frontiers in Marine Science*, *8*. https://doi.org/10.3389/fmars.2021.584445

Frankignoulle, M. (1994). A complete set of buffer factors for acid/base CO2 system in seawater. *Journal of Marine Systems*, *5*(2), 111-118.

Fritsch, F. N., & Carlson, R. E. (1980). Monotone Piecewise Cubic Interpolation. *SIAM Journal on Numerical Analysis*, *17*(2), 238-246. https://doi.org/10.1137/0717021

Fujii, M., Takao, S., Yamaka, T., Akamatsu, T., Fujita, Y., Wakita, M., Yamamoto, A., & Ono, T. (2021). Continuous Monitoring and Future Projection of Ocean Warming, Acidification, and Deoxygenation on the Subarctic Coast of Hokkaido, Japan [Original Research]. *Frontiers in Marine Science*, *8*. https://doi.org/10.3389/fmars.2021.590020

Gattuso, J.-P., Magnan, A., Billé, R., Cheung, W. W., Howes, E. L., Joos, F., Allemand, D., Bopp, L., Cooley, S. R., & Eakin, C. M. (2015). Contrasting futures for ocean and society from different anthropogenic CO2 emissions scenarios. *Science*, *349*(6243), aac4722.

Gruber, N., & Sarmiento, J. L. (2002). Large-scale biogeochemical-physical interactions in elemental cycles. *The Sea*, *12*, 337-399.

Ho, D. T., Law, C. S., Smith, M. J., Schlosser, P., Harvey, M., & Hill, P. (2006). Measurements of air-sea gas exchange at high wind speeds in the Southern Ocean: Implications for global parameterizations. *Geophysical Research Letters*, *33*(16).

Hofmann, G. E., Smith, J. E., Johnson, K. S., Send, U., Levin, L. A., Micheli, F., Paytan, A., Price, N. N., Peterson, B., Takeshita, Y., Matson, P. G., Crook, E. D., Kroeker, K. J., Gambi, M. C., Rivest, E. B., Frieder, C. A., Yu, P. C., & Martz, T. R. (2011). High-Frequency Dynamics of Ocean pH: A Multi-Ecosystem Comparison. *PLOS ONE*, *6*(12), e28983. https://doi.org/10.1371/journal.pone.0028983

Humphreys, M. P., Lewis, E. R., Sharp, J. D., & Pierrot, D. (2022). PyCO2SYS v1.8: marine carbonate system calculations in Python. *Geosci. Model Dev.*, *15*(1), 15-43. https://doi.org/10.5194/gmd-15-15-2022

James, R. K., van Katwijk, M. M., van Tussenbroek, B. I., van der Heide, T., Dijkstra, H. A., van Westen, R. M., Pietrzak, J. D., Candy, A. S., Klees, R., Riva, R. E. M., Slobbe, C. D., Katsman, C. A., Herman, P. M. J., & Bouma, T. J. (2020). Water motion and vegetation control the pH dynamics in seagrass-dominated bays. *Limnology and Oceanography*, *65*(2), 349-362. https://doi.org/https://doi.org/10.1002/lno.11303

Jiang, L.-Q., Carter, B. R., Feely, R. A., Lauvset, S. K., & Olsen, A. (2019). Surface ocean pH and buffer capacity: past, present and future. *Scientific reports*, *9*(1), 1-11.

Johnson, K. S., Riser, S. C., & Karl, D. M. (2010). Nitrate supply from deep to near-surface waters of the North Pacific subtropical gyre. *Nature*, *465*(7301), 1062-1065.

Jokiel, P. L., Jury, C. P., & Rodgers, K. S. (2014). Coral-algae metabolism and diurnal changes in the CO2-carbonate system of bulk sea water. *PeerJ*, *2*, e378. https://doi.org/10.7717/peerj.378

Jones, D. C., Ito, T., Takano, Y., & Hsu, W. C. (2014). Spatial and seasonal variability of the air-sea equilibration timescale of carbon dioxide. *Global Biogeochemical Cycles*, *28*(11), 1163-1178.

Lee, K., Tong, L. T., Millero, F. J., Sabine, C. L., Dickson, A. G., Goyet, C., Park, G. H., Wanninkhof, R., Feely, R. A., & Key, R. M. (2006). Global relationships of total alkalinity with salinity and temperature in surface waters of the world's oceans. *Geophysical Research Letters*, *33*(19).

Li, A., Aubeneau, A. F., King, T., Cory, R. M., Neilson, B. T., Bolster, D., & Packman, A. I. (2019). Effects of vertical hydrodynamic mixing on photomineralization of dissolved organic carbon in arctic surface waters. *Environmental Science: Processes & Impacts*, *21*(4), 748-760.

Liu, X., Patsavas, M. C., & Byrne, R. H. (2011). Purification and characterization of meta-cresol purple for spectrophotometric seawater pH measurements. *Environmental Science & Technology*, *45*(11), 4862-4868.

Longhurst, A. R. (2010). *Ecological geography of the sea*. Elsevier.

Lueker, T. J., Dickson, A. G., & Keeling, C. D. (2000). Ocean pCO2 calculated from dissolved inorganic carbon, alkalinity, and equations for K1 and K2: validation based on laboratory measurements of CO2 in gas and seawater at equilibrium. *Marine Chemistry*, *70*(1-3), 105-119.

Martz, T. R., Connery, J. G., & Johnson, K. S. (2010). Testing the Honeywell Durafet® for seawater pH applications. *Limnology and Oceanography: Methods*, *8*(5), 172-184. https://doi.org/https://doi.org/10.4319/lom.2010.8.172

Middelburg, J. J., Soetaert, K., & Hagens, M. (2020). Ocean Alkalinity, Buffering and Biogeochemical Processes. *Reviews of Geophysics*, *58*(3), e2019RG000681. https://doi.org/10.1029/2019rg000681

Millero, F. J. (2007). The marine inorganic carbon cycle. *Chemical reviews*, *107*(2), 308-341.

Millero, F. J., & Poisson, A. (1981). International one-atmosphere equation of state of seawater. *Deep Sea Research Part A. Oceanographic Research Papers*, *28*(6), 625-629.

Orr, J. C., Fabry, V. J., Aumont, O., Bopp, L., Doney, S. C., Feely, R. A., Gnanadesikan, A., Gruber, N., Ishida, A., Joos, F., Key, R. M., Lindsay, K., Maier-Reimer, E., Matear, R., Monfray, P., Mouchet, A., Najjar, R. G., Plattner, G.-K., Rodgers, K. B.,…Yool, A. (2005). Anthropogenic ocean acidification over the twenty-first century and its impact on calcifying organisms. *Nature*, *437*(7059), 681-686. https://doi.org/10.1038/nature04095

Osborne, E. B., Thunell, R. C., Gruber, N., Feely, R. A., & Benitez-Nelson, C. R. (2020). Decadal variability in twentieth-century ocean acidification in the California Current Ecosystem. *Nature Geoscience*, *13*(1), 43-49. https://doi.org/10.1038/s41561-019-0499-z

Possenti, L., Humphreys, M. P., Bakker, D. C. E., Cobas-García, M., Fernand, L., Lee, G. A., Pallottino, F., Loucaides, S., Mowlem, M. C., & Kaiser, J. (2021). Air-Sea Gas Fluxes and Remineralization From a Novel Combination of pH and O2 Sensors on a Glider [Original Research]. *Frontiers in Marine Science*, *8*(1210). https://doi.org/10.3389/fmars.2021.696772

Price, N. N., Martz, T. R., Brainard, R. E., & Smith, J. E. (2012). Diel Variability in Seawater pH Relates to Calcification and Benthic Community Structure on Coral Reefs. *PLOS ONE*, *7*(8), e43843. https://doi.org/10.1371/journal.pone.0043843

Qu, L., Xu, J., Sun, J., Li, X., & Gao, K. (2017). Diurnal pH fluctuations of seawater influence the responses of an economic red macroalga Gracilaria lemaneiformis to future CO2-

Formatted: French (France)

induced seawater acidification. *Aquaculture*, *473*, 383-388. https://doi.org/https://doi.org/10.1016/j.aquaculture.2017.03.001

Qu, T., & Lindstrom, E. J. (2004). Northward intrusion of Antarctic Intermediate Water in the western Pacific. *Journal of Physical Oceanography*, *34*(9), 2104-2118.

Raven, J. A., & Johnston, A. M. (1991). Mechanisms of inorganic-carbon acquisition in marine phytoplankton and their implications for the use of other resources. *Limnology and Oceanography*, *36*(8), 1701-1714.

Richardson, D. J. (2000). Bacterial respiration: a flexible process for a changing environment. *Microbiology*, *146*(3), 551-571.

Staudinger, C., Strobl, M., Breininger, J., Klimant, I., & Borisov, S. M. (2019). Fast and stable optical pH sensor materials for oceanographic applications. *Sensors and Actuators B: Chemical*, *282*, 204-217. https://doi.org/https://doi.org/10.1016/j.snb.2018.11.048

Staudinger, C., Strobl, M., Fischer, J. P., Thar, R., Mayr, T., Aigner, D., Müller, B. J., Müller, B., Lehner, P., Mistlberger, G., Fritzsche, E., Ehgartner, J., Zach, P. W., Clarke, J. S., Geißler, F., Mutzberg, A., Müller, J. D., Achterberg, E. P., Borisov, S. M., & Klimant, I. (2018). A versatile optode system for oxygen, carbon dioxide, and pH measurements in seawater with integrated battery and logger. *Limnology and Oceanography: Methods*, *16*(7), 459-473. https://doi.org/https://doi.org/10.1002/lom3.10260

Stoll, M., Bakker, K., Nobbe, G., & Haese, R. (2001). Continuous-flow analysis of dissolved inorganic carbon content in seawater. *Analytical Chemistry*, *73*(17), 4111-4116.

Strickland, J. D. H., & Parsons, T. R. (1972). A practical handbook of seawater analysis.

Stumm, W., & Morgan, J. J. (2012). *Aquatic chemistry: chemical equilibria and rates in natural waters*. John Wiley & Sons.

Sutton, A. J., Feely, R. A., Maenner-Jones, S., Musielwicz, S., Osborne, J., Dietrich, C., Monacci, N., Cross, J., Bott, R., Kozyr, A., Andersson, A. J., Bates, N. R., Cai, W. J., Cronin, M. F., De Carlo, E. H., Hales, B., Howden, S. D., Lee, C. M., Manzello, D. P.,…Weller, R. A. (2019). Autonomous seawater pCO2 and pH time series from 40 surface buoys and the emergence of anthropogenic trends. *Earth Syst. Sci. Data*, *11*(1), 421-439. https://doi.org/10.5194/essd-11-421-2019

Takahashi, T., Sutherland, S. C., Feely, R. A., & Wanninkhof, R. (2006). Decadal change of the surface water pCO2 in the North Pacific: A synthesis of 35 years of observations. *Journal of Geophysical Research: Oceans*, *111*(C7).

Tilstone, G. H., Figueiras, F., Lorenzo, L. M., & Arbones, B. (2003). Phytoplankton composition, photosynthesis and primary production during different hydrographic conditions at the Northwest Iberian upwelling system. *Marine Ecology Progress Series*, *252*, 89-104.

Uppström, L. R. (1974). The boron/chlorinity ratio of deep-sea water from the Pacific Ocean. *Deep Sea Research and Oceanographic Abstracts*, *21*(2), 161-162. https://doi.org/https://doi.org/10.1016/0011-7471(74)90074-6

Vallis, G. K. (2017). *Atmospheric and oceanic fluid dynamics*. Cambridge University Press.

Wang, X., Yin, Z., Chen, J., & Liu, J. (2023). Phytoplankton Carbon Utilization Strategies and Effects on Carbon Fixation. *Water*, *15*(11), 2137. https://www.mdpi.com/2073-4441/15/11/2137

Wei, Z., Zhang, Y., Yang, F., & Long, L. (2022). Diurnal fluctuations in seawater pCO2 amplify the negative effects of ocean acidification on the biotic performance of the calcifying

Formatted: French (France)

macroalga Halimeda opuntia [Original Research]. *Frontiers in Marine Science*, *9*. https://doi.org/10.3389/fmars.2022.968740

Williams, R. G., & Follows, M. J. (2003). Physical transport of nutrients and the maintenance of biological production. In *Ocean biogeochemistry: The role of the ocean carbon cycle in global change* (pp. 19-51). Springer.

Wu, Y., Hain, M. P., Humphreys, M. P., Hartman, S., & Tyrrell, T. (2019). What drives the latitudinal gradient in open-ocean surface dissolved inorganic carbon concentration? *Biogeosciences*, *16*(13), 2661-2681. https://doi.org/10.5194/bg-16-2661-2019

Zeebe, R. E., & Wolf-Gladrow, D. A. (2001). *CO2 in seawater: equilibrium, kinetics, isotopes*. http://site.ebrary.com/id/10190754

Zehr, J. P., & Kudela, R. M. (2011). Nitrogen cycle of the open ocean: from genes to ecosystems. *Annual Review of Marine Science*, *3*, 197-225.